Spatiotemporal responses of runoff to climate change on the southern Tibetan Plateau

He Sun[1*], Tandong Yao[1,2], Fengge Su[1,2*], Wei Yang[1,2], Deliang Chen[3]

[1]State Key Laboratory of Tibetan Plateau Earth System, Environment and Resources (TPESER), Institute of Tibetan Plateau Research, Chinese Academy of Sciences, Beijing 100101, China

[2]University of Chinese Academy of Sciences, Beijing 100101, China

[3]Regional Climate Group, Department of Earth Sciences, University of Gothenburg, Gothenburg 405 30, Sweden

*Corresponding author: He Sun, Fengge Su

State Key Laboratory of Tibetan Plateau Earth System, Resources and Environment, Institute of Tibetan Plateau Research, Chinese Academy of Sciences, Beijing 100101, China

Email: sunhe@itpcas.ac.cn, fgsu@itpcas.ac.cn

Abstract

A comprehensive understanding of spatiotemporal runoff changes at a sub-basin scale of the Yarlung Zangbo (YZ) basin on the southern Tibetan Plateau (TP), amidst varying climatic and cryospheric conditions, is imperative for effective water resources management. However, spatiotemporal differences of runoff composition, change and the attribution within the YZ basin have not been extensively explored, primarily due to the lack of hydrometeorological observations, especially in the downstream region. In this study, we investigated historical and future evolution of annual and seasonal total water availability, as well as glacier runoff and snowmelt contributions across six sub-basins of the YZ with a particular focus on the comparison between the upstream Nuxia (NX) basin and the downstream Nuxia-Pasighat (NX-BXK) basin, based on a newly generated precipitation dataset and a well-validated model with streamflow, glacier mass, and snow cover observations. Our findings revealed large spatiotemporal differences in changes exist within the YZ basin for 1971–2020. Firstly, runoff generation was dominated by rainfall runoff throughout the YZ basin, with glacier runoff playing more important role in the annual total runoff (19%) in the NX-BXK sub-basin compared to other sub-basins. Notably, glacier runoff contributed 52% of the total runoff at the Pasighat outlet of the YZ basin. Secondly, annual runoff exhibited an increasing trend in the NX basin but a decreasing trend in the NX-BXK, primarily attributed to rainfall runoff changes influenced by atmospheric moisture. Glacier runoff enhanced water supply, by offsetting the decreasing contribution from rainfall. Total runoff will consistently increase (27–100 mm/10yr)

across the sub-basins through the 21st century, resulting from increased rainfall runoff and a minor effect of increased snowmelt and glacier runoff.

Keywords

Runoff Composition; Runoff Changes; VIC-Glacier Hydrological Model; Yarlung Zangbo; Tibetan Plateau

Highlights

- Runoff generation is dominated by rainfall runoff (59%–72%) in the YZ, and the largest glacier runoff contribution is in the downstream sub-basin (16%–19%).
- Annual runoff trends indicate an increase in the NX but a decrease in the NX-BXK for 1971–2020, due to contrasting precipitation changes.
- Total runoff across the sub-basins will consistently increase (27–100 mm/10yr) through the 21st century, mostly resulting from increased rainfall runoff.

1 Introduction

Climatic and cryospheric changes have profoundly affected hydrological processes in high-mountain regions. The Tibetan Plateau (TP), konwn as the Asian Water Tower, supplying freshwater to nearly 2 billion people. Marked atmospheric warming since the 1980s has changed the balance between liquid and solid states of water, leading to shifts in river runoff, glacier, and snow melt dynamics (Yao et al. 2022). These drastic changes in the upper mountains of the TP pose a threat to the sustainability of the downstream water supply.

The Yarlung Zangbo (YZ, Figure 1) river basin, located in the southern TP is the largest river basin of the TP and a vital freshwater source for the Tibet Autonomous Region (TAR). It constitutes the main agricultural region in the TAR (Yang et al., 1989; Zhong et al., 2014). Like elsewhere on TP, a rapid ongoing temperature rise (0.3–0.4°C per decade) since the mid-1960s potentially influences runoff processes and water resources availability in the YZ basin (Yao et al., 2012; Li et al., 2018). The YZ basin, spanning approximately 250,000 km², exhibits diverse climatic systems, including the Indian summer monsoon and the westerly system, and varying glacier and snow conditions (Zhang et al., 2013). These factors contribute to spatiotemporal differences in runoff changes within the YZ basin. Therefore, gaining a comprehensive understanding of runoff regimes and flow changes at the sub-basin scale is crucial for informed decision-making in water resources management and social development.

While numerous studies have investigated runoff regimes and changes using hydrological models in the YZ basin, most have focused solely on the region upstream of the Nuxia (NX) hydrological station (Figure 1, Table 1) (Chen et al., 2017; Cuo et al., 2019; Su et al., 2016; Zhang et al., 2013; Zhao et al., 2019; Cui et al., 2023; Gu et al., 2023). This focus is due to the nearest national hydrological station's proximity to the mainstream outlet, providing long-term daily records (> 50years). Conversely, the glacierized downstream region (about 65% of the total glacier area in the YZ), particularly between NX and Pasighat outlet (NX-BXK, Figure 1) has received less attention. This lack of focus is attributed to limited hydrometeorological and glacier observations in this sub-basin. Remarkably, this region exhibits the largest glacier retreat in the TP, with a length reduction rate of 48.2m yr^{-1} and an area decrease of 0.57% yr^{-1} during the 1970s–2000s (Yang et al., 2013; Yao et al., 2012). These changes have the potential to significantly alter the runoff regime, influencing the quantity, timing, and variability of flows across space and time. However, the characteristics and changes in runoff, along with the effect of glacier melt on water supply, remain unclear in the NX-BXK sub-basin.

The NX basin, with an area of approximately 201,548 km^2, presents divergent glacier and snow conditions (Table 2). For example, the region upstream of the Lhatse hydrological station (Figure 1), the source region of the YZ river, is influenced by both monsoon and westerlies, experiencing higher precipitation in spring and winter compared to other NX sub-basins (Figure S1 in Supporting Information). The Lhasa (LS) and Rikaze (RKZ) sub-basins, vital crop centers

for the central Tibet Autonomous Region, play a crucial role in irrigation water resources. The LS sub-basin, with about 23% snow cover contrasts with the RKZ sub-basin, which has little glacier and snow coverage (Table 2). This difference suggests that the water supply in the RKZ sub-basin is more sensitive to climate change. Moreover, runoff in the region between Yangcun and NX hydrological stations (YC-NX, Figure 1) contributes 51% to the total runoff at the NX hydrological station (Sun and Su, 2020), making runoff regimes and changes in this sub-basin influential for the entire NX basin. Therefore, a comprehensive investigation into runoff regimes and changes in different sub-basins is essential for a nuanced understanding of the mechanisms underlying runoff changes in response to climate change.

While many hydrological studies focus on the region upstream of the NX hydrological station (Zhang et al., 2013; Lutz et al., 2014; Zhao et al., 2019; Sun and Su, 2020; Khanal et al., 2021; Nan et al., 2021; Wang et al., 2021), considerable differences in runoff regimes and change studies exist in the NX basin (Table 1). These differences may arise from variations in forcing inputs for hydrological model simulations. Accurate precipitation inputs play an important role in reliable hydrological model simulations. However, high mountain precipitation in the YZ basin is still inadequately represented in gauge-based, satellite-based, and reanalysis-based estimates, or outputs of regional climate models (Wang and Zeng, 2012; Liu et al., 2020; Sun et al., 2021). The mean annual precipitation ranges from 360–1236 mm in the YZ basin (Qi et al. 2018; Sun; Su 2020; Tong et al. 2014), resulting in significant uncertainties in hydrological

simulations. This inconsistency in gridded datasets is often underestimated in hydro-climate studies, especially in glacierized basins with limited data coverage. Even when realistic runoff simulations are achieved at the catchment outlet, they cannot guarantee reasonable results (Zhao et al., 2019) due to the compensation between precipitation-induced runoff and snow/glacier melting. For example, Lutz et al. (2014) simulated glacier runoff in the NX basin with the Spatial Processes in HYdrology (SPHY) model driven by the Asian Precipitation-Highly-Resolved Observational Data Integration Towards Evaluation (APHRODITE) precipitation estimates, suggesting that glacier runoff contributed about 16% to total runoff. In contrast, Khanal et al. (2021) proposed that glacier runoff contributed about 1.8% to total runoff with the same model driven by the newly released fifth-generation reanalysis (ERA5) precipitation of the European Centre for Medium-Range Weather Forecasts (Table 1), primarily due to the overestimation of the ERA5 precipitation estimate. Sun and Su (2020) indicated that the contribution of glacier runoff would increase by 7–10% with a unit decrease in mean annual precipitation. Therefore, an accurate precipitation estimate is crucial as a model input to simulate runoff regimes, and further quantify the effect of glaciers and snowmelt on runoff in the NX basin.

These uncertainties in the hydrological simulation will be introduced and enlarged on the uncertainty in future projections (Lutz et al. 2016). Existing studies of hydrological responses to future climate changes have been a debate in the NX sub-basin of the YZ basin. For example,

Lutz et al. (2014) forced the Spatial Processes in Hydrology (SPHY) model using outputs from 4 global climate models (GCMs) and showed that runoff would be increased by 3–13% relative to the reference period 1998–2007 until at least 2050s due to the increasing precipitation in the YZ basin. Zhao et al. (2019) projected the future runoff changes with 5 GCM outputs using an extended Variable Infiltration Capacity (VIC) macroscale hydrological model (VIC-CAS), suggesting that the total runoff will increase by 16–31% by the end of this century relative to the reference period 1970–2010 because of increased rainfall-induced runoff in the YZ basin. Cui et al. (2023) also suggested that total runoff in the YZ basin will increase of 7.3±11% by 2070s relative to the 1985–2014 resulted from rainfall runoff. Meanwhile, Su et al. (2016) projected a runoff increase of 6.7–14.4% in the 2041–2070 relative to the reference period 1971–2000 in the YZ forced by the VIC-Glacier model with ensemble outputs of 20 GCMs, and attributed the runoff increases to the rising glacier melt runoff. In addition, future flow evolution and the effect of different runoff compositions on total runoff in the NX-BXK are also unclear.

To address these issues, this study divided the YZ into six sub-basins and collected streamflow observations at three hydrological stations (Yigong, Bomi, and Motuo) and glacier mass balance observations (Parlung No.94) in the NX-BXK sub-basin, filling in the gap of scarce data coverage. Additionally, streamflow observations at five national hydrological stations and glacier mass balance observations at a site (Gurenhekou) in the five sub-basins of the NX

(Figure 1), together with hydrological stations in the NX-BXK, constitute a unique observation basis. This basis allows us to validate the glacier-hydrology model and reveal runoff regimes, and changes at the sub-basin scale. Precipitation observations at 280 gauges, were collected, and a high spatiotemporal resolution (10 km; daily) precipitation dataset was generated using a machine learning algorithm based on these gauges (Sun et al., 2022).

Leveraging this basin-wide observation dataset, this study comprehensively investigates runoff compositions, changes, and attributions across six sub-basins in the YZ for 1971–2020, with a particular focus on the comparison between the NX and NX-BXK. This investigation employs the process-based and well-established Variable Infiltration Capacity (VIC)-Glacier hydrological model. Furthermore, the study assesses the future evolution of annual and seasonal total water availability, glacier runoff, and snowmelt, using an ensemble of multiple global climate models (GCMs) from the latest release of the Coupled Model Intercomparison Project Phase 6 (CMIP6). The objectives are to: (1) use the model framework to identify spatiotemporal characteristics in runoff compositions and changes at the sub-basin scale under heterogeneous climate and glacier/snow conditions. (2) quantify the contributions of three major runoff compositions (glacier, rainfall, and snowmelt runoff) to total runoff among different sub-basins, and investigate their responses to climate changes. (3) assess future water availability under 21st-century climate-cryosphere change, assisting policy-makers and water managers in adopting strategies. These findings are anticipated to provide a basic framework for studying

cryospheric basin hydrological cycles in the TP and provide adaptation strategies for rational water resource management, and social, and economic development grounded in a robust scientific understanding.

2 Study Area

In this study, the YZ basin is divided into six sub-basins based on flow direction and locations of hydrological stations (Figure 1; Table 2). There are five sub-basins located upstream of the Nuxia (NX) hydrological station, collectively termed the NX basin, with an additional sub-basin lying between Nuxia and Pasighat (NX-BXK) hydrological stations. The NX basin comprises the upstream sub-basins of Lhatse (LZ), Shigatse (RKZ), and Lhasa (LS) hydrological stations, along with the sub-basins between Lhatse and Yangcun (LZ-YC) hydrological station and between Yangcun and Nuxia (YC-NX) hydrological station.

The climate in the YZ is characterized by a wet and warm summer and a cool, dry winter, with precipitation mostly dominated by the summer monsoon, contributing 70–90% of annual totals during June–September (Figure S1). Furthermore, mean annual precipitation increases downstream in the YZ basin, ranging from 283 mm upstream to 1465 mm downstream, averaging about 774 mm for the entire YZ basin (Table 2). All sub-basins exhibit similar seasonal temperature patterns, with peaks mainly occurring in July–August (Figure S1). Glacier coverage varies from 0.9% (LZ-YC) to 10.2% (NX-BXK), averaging 3.3% for the entire YZ

basin. The YC-NX (2.8%) and NX-BXK (10.2%) sub-basins host the most extensive glacier coverage (Table 1). The mean annual snow cover fraction (SCF) ranges from 7% (RKZ) to 32% (NX-BXK), with an average of 19% across the YZ basin.

3 Data and Method

3.1 Data

Daily precipitation, maximum and minimum temperature, and wind speed estimates with a spatial resolution of 10×10 km were used as the VIC-Glacier model forcing inputs in this work. Historical meteorological data during 1971–2100 was adopted from Sun et al. (2022). The daily precipitation data with a spatial resolution of 10×10 km for 1961–2020 was reconsructed by correcting gridded estimates from the ERA5 precipitation of the European Centre for Medium-Range Weather Forecasts (ECMWF) based on 580 rain gauges in the monsoon-dominated TP region (290 rain gauges in the YZ basin, Figure 1) and the Random Forest-based (RF) machine learning algorithm (Sun et al., 2022). Inputs of the RF algorithm selected in this study include: 1) geographical features (e.g., longitude, latitude, elevation, slope gradient and aspect), which influence precipitation distribution, and 2) climatic features derived from the ERA5 (e.g., convective available potential energy, lifting condensation level, and total column water vapor), which represent the potential for the generation and development of precipitation. The corrected precipitation data set was evaluated at a point scale by comparing it with gauge observations, and has been inversely evaluated by the hydrological model, which demonstrates its suitability

for hydrological simulation (Sun et al., 2022). It was downloaded from the National Tibetan Plateau/Third Pole Environment Data Center (TPDC, https://doi.org/10.11888/Atmos.tpdc.272885).

Using the newly generated daily meteorological data for 1961–2020, Sun et al. (2024) applied the Bias Corrected Spatial Disaggregation (BCSD) statistical downscaling approach (Wood 2002; Wood et al. 2004) to downscale and bias-correct daily transient meteorological data, including precipitation, maximum and minimum temperature, and wind speed, with a spatial resolution of 10×10 km through the 21st century from 10 GCMs from the CMIP6 under the Shared Socioeconomic Pathways (SSPs)2-4.5 and SSP5-8.5 scenario. Daily transient climate estimates, at a spatial resolution of 10×10 km for 1971–2100 under 20 scenarios (10 GCMs × 2 SSPs) from Sun et al. (2024) were directly employed to drive the VIC-Glacier model to continuous runoff production in the YZ basin.

Observed streamflow, observed glacier mass balance, satellite-based glacier area and snow cover fraction estimates were applied to calibrate and validate the model in this study. Monthly streamflow since 1971 were collected at eight hydrological stations (Lhatse, Shigatse, Lhasa, Yangcun, Nuxia, Yigong, Bomi, and Motuo from the Ministry of Water Resources, China (Figure 1, Table S1).

Two shapefiles of glacier inventory, the first Glacier Inventory of China (CGI) from the "Environment & Ecological Science Data Center for west China" (http://westdc.westgis.ac.cn/glacier) and Randolph Glacier Inventory (RGI) 6.0 (https://www.glims.org/RGI/rgi60_dl.html), were used to describe the glacier information of the YZ in the VIC-Glacier model. Observed annual glacier mass balance data from Gurenhekou and Parlung No.94 glacier sites since 2005 were used to validate the performance of glacier model (http://www.tpdc.ac.cn, Figure 1, Table S1). The Moderate Resolution Imaging Spectroradiometer (MODIS) 10CM reporting the maximum percentage of snow cover during an 8-day period in 0.05° resolution grid (https://nsidc.org/ data) during 2006–2018 was used to calculate the snow cover fraction (SCF) and to compare with VIC-Glacier model simulations in the YZ basin.

The model required land surface characteristics, including soil texture and vegetation types, were adopted from Sun and Su (2020). These data were used as initial model inputs, and remained unchanged in simulation period.

3.2 VIC-Glacier Hydrological Model

The present study employed the physically-based and distributed VIC hydrological model (Liang et al., 1994; Liang et al., 1996) linked with a simple degree-day glacier melt algorithm (Hock, 2003), referred to as VIC-Glacier. This modeling framework facilitates the

comprehensive simulation of the physical exchange of water and energy within a grid mesh encompassing soil, vegetation, and the atmosphere. The VIC-Glacier effectively models surface water balance compositions, including evapotranspiration, surface runoff, baseflow (subsurface drainage into the local stream channel network, as opposed to groundwater recharge), and total soil moisture, including liquid and ice content in each soil layer. The model integrates a two-layer energy-balance snow model (Cherkauer and Lettenmaier, 1999) and a frozen soil/permafrost algorithm (Cherkauer and Lettenmaier, 1999; 2003). These components account for ground snowpack, snow within the vegetation canopy, snow atop lake ice, and sublimation of snow. In each time step, the model calculates the rain or snow fraction contributing to the snowpack. Subsequently, all energy fluxes are computed, triggering melt if the energy balance is positive. The VIC-Glacier model has demonstrated its effectiveness in hydrological simulations for various high-mountainous TP basins (Meng et al., 2019; Su et al., 2016; Sun and Su, 2020; Tong et al., 2016; Zhang et al., 2013; Zhao et al., 2019).

Here, the modeling framework at a 10 km ×10 km spatial resolution and a three-hourly time step was adopted from Sun and Su (2020). To categorize the total runoff sources in this study, we partitioned it into three components: rainfall runoff, snowmelt runoff, and glacier runoff. Glacier runoff was defined as all water generated in the glacierized area, including rainfall, snow melt, and ice melt in the glacierized area.

282 $$Total\ runoff\ (TR) = Rainfall\ runoff\ (RR) + Snowmelt\ runoff(SR) +$$

283 $$Glacier\ runoff(GR) \quad (1)$$

284 $$Rainfall\ runoff\ contribution = \frac{RR}{TR} \times 100\% \quad (2)$$

285 $$Snowmelt\ runoff\ contribution = \frac{SR}{TR} \times 100\% \quad (3)$$

286

287 Recognizing the influence of glacier melt at different elevations, each glacierized grid cell
288 underwent division into various elevation bands with an interval of 100 m (Kan et al., 2018).
289 The simulated total runoff of each grid is from both the glacierized and non-glacierized areas,
290 that is,

291 $$R_i = f \times R_{glac} + (1 - f) \times R_{vic} \quad (4)$$

292 Where, R_i is the total runoff (mm) in grid *I*, *f* is the percentage of glacier area, and glacier area
293 is updated every year, R_{glac} is the runoff (mm) from the glacier area calculated by the glacier
294 model, and R_{vic} is the sum of surface runoff and baseflow runoff (mm) for non-glacierized areas
295 calculated by the VIC model, including both rainfall and seasonal snowmelt runoff. R_{glac} can
296 be calculated as:

297 $$M_i = \begin{cases} DDF \times (T - T_{base}); T > T_{base} \\ 0; \qquad\qquad T \leq T_{base} \end{cases} \quad (5)$$

298 $$R_{glac} = M_1 + M_2 + \cdots + M_i; i = 1, 2, 3, \ldots, n \quad (6)$$

299 where, M_i is the meltwater (mm) from elevation band *j* and *n* is the total number of elevation
300 bands in grid *i*; *DDF* is the degree-day factors of glacier or snow melt (mm °C^{-1} day^{-1}); *T (°C)*
301 is the daily average air temperature above the glacier surface; T_{base} (°C) is the temperature
302 threshold for glacier and snow melt (0 °C). In a precipitation event, rainfall occurs when the air

303 temperature is above 0°C; otherwise, it snows. In the presence of a snowpack on the glacier,
304 the snow melts first before glacier melting starts, following the same degree-day approach but
305 different degree-day factors.
306
307 The calculated glacier area and volume were updated every year in the model by the volume-
308 area scaling approach (Bahr et al., 1997). An exponential form (equation 7), derived from
309 glacier observations in western China (Liu et al., 2003), converts glacier area to volume for a
310 basin:

311 $$V = 0.04S^{1.35} \quad (7)$$

312 Where, V is glacier volume (km^3) and S is glacier area (km^2). Initial glacier volume was
313 determined using glacier area data from the first Glacier Inventory of China (CGI V1.0,
314 http://westdc.westgis.ac.cn/glacier) dataset, which presented glacier area for period
315 1970s−1990s. The Randolph Glacier Inventory (RGI V6.0) dataset presented glacier area for
316 period 2000s−2010s. Therefore, glacier area was simulated by glacier model since 1971, and
317 then it was updated every year with the snowfall accumulation and simulated ice melt from all
318 the glacier cells in the glacier model based on volume-area scaling approach. The simulated
319 mean annual glacier area during 2000−2010 was compared with the Randolph Glacier
320 Inventory (RGI V6.0) dataset in the YZ basin and its six sub-basins.
321
322 **3.3 Model Calibration and Validation**
323 The VIC-Glacier model requires the calibration of two sets of parameters: (1) the degree day
324 factor (DDF), related to glacier runoff simulation; and (2) VIC model parameters related to

runoff simulation in non-glacierized regions. The latter includes parameters (Table 3) such as the depth of the first and second soil layers (D1 and D2), the infiltration shape parameter (B_inf), and three base flow parameters, including the maximum velocity of baseflow (Dsmax), a fraction of Dsmax where non-linear baseflow begins (Ds), and a fraction of maximum soil moisture where non-linear baseflow occurs (Ws).

To adjust the internal stores of energy and water from the initial state to equilibrium, the VIC-Glacier model underwent a spin-up from 1961–1970, with subsequent simulation for the years 1971–2020. In addition, 1971–2000 was selected as the calibration period and 2001–2015 the validation period based on the observed monthly streamflow for 1971–2015. Calibration and validation of the VIC-Glacier hydrological model followed a systematic two-step approach, employing observed streamflow, glacier mass balance, and satellite-based estimates of glacier area and snow cover fraction (Table S1). Model performance was assessed using metrics such as Nash-Sutcliffe efficiency (NSE), relative bias (RB, %), and correlation coefficient (CC). The optimization process utilized a trial-and-error method to minimize bias against predefined criteria. Linear regression was employed to calculate annual and seasonal trends of precipitation, temperature, and runoff.

The model calibration and validation were conducted using a two-step approach to overcome equifinality problems. First, initial values of DDF parametersin the glacier model related to

345 glacier and snowmelt were adopted from Sun and Su (2020). The glacier model was calibrated
346 to match the glacier area observations from RGI V6 for 2000s−2010s in the YZ and six sub-
347 basins, and validated by observed mass balance data from the Gurenhekou site in the NX basin
348 and the Parlung No.94 glacier site in the NX-BXK sub-basin (Figure S2). Given the good
349 performance in simulating glacier area (with RB of mostly < 7%, Figure 2c) and good
350 consistency (CCs of 0.65–0.96) in annual variations between observed glacier mass balance
351 and simulation, final DDF values (6.5–11.0 $mm°C^{-1}$ day^{-1}) were determined across six sub-
352 basins (Table 3).
353
354 Second, the VIC-related parameters were validated against observed streamflow and satellite-
355 based snow cover fraction (SCF) data. The infiltration parameter (B_inf) and the second soil
356 layer depth (D2) have been identified as the most sensitive parameters (Zhang et al., 2013). The
357 B_inf which defines the shape of the variable infiltration capacity curve has a common range
358 of 0–0.4, while the D2 mainly determines the moisture storage capacity of the VIC model, with
359 a range of 0.5–1.0 (Liang et al., 1996; Shi et al., 2008). The simulated monthly streamflow
360 captured well the magnitudes and patterns of observation at eight hydrological stations, with
361 NSEs of 0.71 to 0.86 and RBs of within ±8% for the calibration and validation period across
362 the sub-basins (Table 3, Figure S3). To further validate the model, monthly satellite-based SCF
363 data for the years 2001–2019 in the YZ basin were compared with the model simulations
364 (Figure S4). The simulated SCF closely mirrors the monthly variations observed in the satellite-

based data, exhibiting a CC of 0.60–0.82 ($p < 0.05$) and RB within ±12% across sub-basins. This alignment suggests the VIC-Glacier model's satisfactory performance in simulating snow cover dynamics in the YZ basin.

4 Result

4.1 Hydrological Response to Historical Climate Changes

4.1.1 Runoff Composition

The credibility of our model allows for a reasonable interpretation of the current runoff composition and change, and their responses to climate change. Examining simulated streamflow across sub-basins reveals significant differences in each sub-basin contribution to the total runoff at the Pasighat outlet of the YZ basin (Figure 1b). The NX-BXK emerges as the most critical runoff-generating area, contributing approximately 52% to the total runoff in the YZ basin, followed by YC-NX (25%), LS (10%), and other sub-basins with contributions ranging from 3% to 6%.

According to the source of runoff generation, total runoff is partitioned into three compositions in this study: rainfall runoff, snowmelt runoff, and glacier runoff. In this study, glacier runoff is defined as all water generated in the glacierized area, including rainfall, snow melt, and ice melt in the glacierized area. Rainfall and snowmelt runoff are originating from the non-glacierized area. Different runoff regimes of rainfall runoff, snowmelt, and glacier runoff influence their contributions to total runoff across the six sub-basins of the YZ with heterogeneous surface

386 characteristics (Figure 2). Rainfall runoff dominates the mean annual total runoff in the YZ and
387 all its sub-basins from 1971 to 2020, contributing 59%–78% to annual total runoff, with an
388 average of 62% in the entire YZ basin. Snowmelt contributes 22% to annual total runoff in the
389 YZ basin, varying from 14% to 36% across six sub-basins, with the LS sub-basin having the
390 largest contribution at 36%. Glacier runoff contributes 16% to the annual total runoff in the YZ
391 basin, ranging from 5% to 19% across six sub-basins for 1971–2020. The highest contributions
392 are in the NX-BXK (19%) and YC-NX (16%) sub-basins, which have the largest glacier
393 coverage in the YZ basin (Table 2).
394
395 Figure 3 shows the spatial pattern of average annual rainfall runoff, snowmelt, and glacier
396 runoff for 1971–2020, along with their percentages at different elevation bands in the YZ basin.
397 The spatial pattern of average annual rainfall runoff (Figure 3a) is similar to that of total runoff
398 (Figure 1b) and precipitation (Figure 3b), decreasing from east to west, with the NX-BXK sub-
399 basin exhibiting the largest runoff. Similarly, the largest snowmelt and glacier runoff occur in
400 the NX-BXK sub-basin, consistent with the spatial distribution of glacier and snow cover area,
401 constituting about 65% of total glacier area and 34% of total snow coverage in the YZ (Figure
402 3c–f). Approximately 84% of the YZ basin runoff originates from middle altitudes (3500–5500
403 m), with 62% from 4500–5500 m and 22% from above 3500–4500 m, primarily contributed by
404 rainfall and seasonal snow (80%–83%, Figure 3g). About 8% of the basin runoff is generated
405 from high altitudes (>5500 m), where 29% of the flow is from glacier runoff, and the remainder

is from rainfall (50%) and snowmelt (21%). In low altitudes (<3500 m), 8% of the basin runoff is primarily from rainfall (82%) and snowmelt (11%), with only 7% attributed to glacier runoff.

The seasonal pattern of total runoff remains consistent across the six sub-basins within the YZ for 1971–2020, with more than 60% of the annual total runoff occurring in June–September and 10%–15% in November–February (Figure 2a–h). This seasonal pattern aligns with the rainfall runoff, which peaks in July–August, reflecting the peak in total runoff in the YZ and its sub-basins (Figure 2 a–h). Snowmelt predominantly takes place from April–October, with peak months varying across sub-basins. In LZ, RKZ, LS, and LZ-YC sub-basins, the peak is in July–September (Figure 2a–d), attributed to the melting of fresh snowfall in the warm season. Conversely, in the YC-NX (Figure 2e) and NX-BXK (Figure 2f) sub-basins, the peak is in May–June, possibly due to snowfall accumulation during October–March. Simulated glacier runoff occurs mainly from June to September for all basins, peaking in July–August, coinciding with the co-occurrences of peak precipitation and temperature.

4.1.2 Runoff Changes and the Response to Climate Changes

(a) Annual Scales

Figure 4 illustrates annual trends in precipitation, temperature, total runoff, and three runoff compositions (rainfall, glacier, and snowmelt runoff) across the six sub-basins for 1971–2020, respectively. Annual variations for precipitation, temperature, and simulated runoff in each sub-

426 basin are presented in Figure S5–S10. All sub-basins exhibit significant warming trends (0.3–
427 0.5 °C/10yr, $p<0.05$), with precipitation tending to increase (6–15 mm/10yr) in the LZ, LZ-YC,
428 LS, RKZ, and YC-NX sub-basins (Figure 4a–e) upstream of the NX hydrological station (NX
429 basin). Conversely, the NX-BXK sub-basin experiences a significant decrease in precipitation
430 (-35 mm/10yr, $p<0.05$, Figure 4f).
431
432 Simulated annual total runoff demonstrates increasing trends of 8.1–18.8 mm/10yr for 1971–
433 2020 across all sub-basins within the NX basin, except for the RKZ sub-basin with an
434 insignificant change (-1.1 mm/10yr), resulting in a significantly increasing trend of 9.4
435 mm/10yr ($p<0.05$) over the entire NX basin (Table 4). Strong correlations between annual
436 variation of total runoff, precipitation, and rainfall runoff exist in these sub-basins (CC of 0.90–
437 0.99, $p<0.05$), while total runoff shows weak relationships with temperature and glacier runoff.
438 This suggests the predominant role of rainfall runoff from nonglacierized areas, with minor
439 impacts from glacier runoff on annual runoff, along with significant increases in precipitation
440 and temperature (Figure 4a). In contrast, the NX-BXK sub-basin exhibits a significantly
441 decreasing trend of 9.4 mm/10yr ($p<0.05$) for 1971–2020 (Figure 4f), resulting from significant
442 decreases in rainfall runoff (-22 mm/10yr) and seasonal snowmelt (-5.5 mm/10yr) from non-
443 glacierized areas. Glacier runoff, however, exhibits a significantly increasing trend (6.0
444 mm/10yr, $p<0.05$, Table 3) in NX-BXK during the same period, partially compensating for the
445 decreasing trend of total runoff in this sub-basin. The integrated result is a weakly increasing

trend of 3.1 mm/10yr in total runoff for the entire YZ basin (Table 4), primarily attributed to increases in rainfall (3.0 mm/10yr) and glacier runoff (2.1 mm/10yr). Snowmelt tends to decrease (-1 to -6 mm/10yr) in the YZ and its sub-basins during 1971–2020, associated with a reduction in solid precipitation and an increase in liquid precipitation (Figure S12), along with significant temperature increases.

Cuo et al. (2019) investigated precipitation and streamflow mutations in the YZ basin using Mann-Kendall analysis, identifying a streamflow mutation in 1997 at the NX hydrological station. This abrupt change is consistent with our long-term runoff observations. This abrupt change is consistent with our long-term runoff observations. Total runoff trends are opposite before and after the year 1998 in the YZ, and its NX and NX-BXK sub-basins (Table 4). During 1971–1997, annual total runoff shows increasing trends (8.9–48.1 mm/10yr) in the basins during 1971–1997, mainly due to an increasing trend in rainfall and glacier runoff (Table 4). However, during 1998–2020, total runoff showed insignificant decreasing trends (-0.3 to -3.3 mm/10yr), attributed to a decreasing trend in rain runoff induced by the weakening Indian monsoon from 1998–2000 (Table 4). It is noteworthy that the rate of decrease in precipitation is faster in NX-BXK (-16.0 mm/10yr) than in NX (-7.0 mm/10yr, Table 4). However, the decline in total runoff is less pronounced in NX-BXK (-0.3 mm/10yr) compared to NX (-3.3 mm/10yr, Table 3) during 1998–2000. This discrepancy arises from different influences of glacier runoff on total runoff between NX and NX-BXK sub-basins. A more rapid increase in glacier runoff

in NX-BXK (16 mm/10yr) than in NX (0.7 mm/10yr, Table 4) partly compensates for the quicker decline in rainfall-runoff, resulting in a slower overall decrease in total runoff in NX-BXK.

Figure 5 illustrates the mean monthly vertical integral of atmospheric moisture budget in June, July, August, and September from ERA5 data across the YZ basin for 1971–2020. It demonstrates an increasing trend in the NX basin but a decreasing trend in the NX-BXK. This pattern corresponds with precipitation trends in the NX and NX-BXK sub-basins, influencing rainfall runoff in these areas. Additionally, teleconnection indices can modulate circulation patterns over a region, thereby affecting precipitation and its induced runoff. Among the 10 teleconnection indices (Text S1), Pacific Decadal Oscillation (PDO) and El Niño/Southern Oscillation (ENSO) exhibit significantly negative consistency with precipitation, while Atlantic Multidecadal Oscillation (AMO) shows significantly positive consistency ($CC=0.43$, $p<0.05$) with precipitation for 1971–2020 in the NX basin (Figure S13a, d). The change in runoff induced by precipitation is mostly influenced by EASM with significantly positive consistency ($CC=0.38$, $p<0.05$) for 1971–2020 in the NX-BXK sub-basin (Figure S13a, e). The streamflow mutation in 1997, associated with the precipitation mutation, is also influenced by NAO and ENSO in the NX and EASM in the NX-BXK.

(b) Seasonal Scales

Because of the similarity in annual runoff regimes and changes across five sub-basins within the NX basin, here, we particularly focus on comparing the NX and NX-BXK sub-basins at seasonal scales for 1971–2020. The high-altitude NX basin exhibits faster warming trends (0.2–0.5 °C/10yr) in each season compared to the low-altitude NX-BXK basin (0.16–0.23 °C/10yr, Figure 6d) for 1971–2020. Seasonal precipitation trends increase (2–9 mm/10yr) for 1971–2020 in the NX basin (Figure 6a), particularly in summer, influenced mainly by the AMO and PDO (Figure S14). Conversely, in the NX-BXK, precipitation decreased (-18 to -2 mm/10yr) for 1971–2020, influenced by the EASM in summer and the AMO in autumn. Consequently, total runoff during 1971–2020 reflects similar trends to precipitation, affected by increased rainfall (1–6 mm/10yr) and glacier runoff (1 mm/10yr) in the NX (Figure 6a), and decreased rainfall (-10 to -3 mm/10yr) and snowmelt (-2 mm/10yr), along with increased glacier runoff (1–5 mm/10yr) in the NX-BXK (Figure 6b). Due to these different trends in the two sub-basins, total runoff shows an increasing trend in summer (5 mm/10yr) but decreasing trends (-1 mm/10yr) in other seasons for 1971–2020 in the YZ basin (Figure 6c), attributed to the dominance of rainfall runoff.

Relative to the period 1971–1997, divergent seasonal changes in total runoff are apparent in the YZ basin during 1998–2020 (Figure 7). In the NX basin, total runoff tends to increase by about 5%–22% in all seasons, with the largest increases during May–August (11%–22%), mainly due

505 to increases in rain-induced and glacier runoff. The smallest increases occur during December–
506 February (5%–6%), mostly due to increased rainfall runoff (3%–5%) in the NX (Figure 7a, d;
507 Table S2). Snowmelt significantly increases during March–May (24%–50%) due to early snow
508 melting (Figure 7d; Table S2), potentially benefiting agricultural water supplies. Conversely,
509 total runoff in the NX-BXK sub-basin decreases by about 3%–20% in all seasons (Figure 7b;
510 Table S2) due to declines in rainfall runoff (3%–23%) and seasonal snowmelt (4%–28%). This
511 indicates a trend toward drier conditions, although increased glacier runoff (2%–12%)
512 somewhat compensates for the loss of total runoff in July–August (Figure 7e). The integrated
513 result of seasonal runoff changes in NX and NX-BXK shows total runoff in the YZ increases
514 by 2%–4% in June–September, mostly due to increases in rain-induced (3%–7%) and glacier
515 runoff (2%–6%), while it decreases in other months due to decreased rain-induced runoff (2%–
516 8%) and seasonal snowmelt (3%–10%, Figure 7c, f, Table S2).
517
518 The distinct seasonal changes in rainfall, snowmelt, and glacier runoff largely play a crucial
519 role in determining the seasonal shifts in their contributions to total runoff across the entire YZ
520 basin and its NX and NX-BXK sub-basins. Compared to the period 1971–1997, the contribution
521 of rainfall increases by 5%–8% from May to October in the NX for 1998–2020, whereas glacier
522 and snowmelt contributions decline by -0.3% to -2% and -5% to -7%, respectively (Figure 7g,
523 Table S2). Conversely, in the NX-BXK, contributions from rainfall runoff and snowmelt
524 decrease by -2% to -6% during May–October, while glacier contribution increases by 2%–7%

525 in these months (Figure 7h, Table S2), underscoring the growing significance of this season in
526 sustaining summer water supplies in the NX-BXK. Taken together, for the entire YZ basin
527 (Figure 7i), glacier contribution increases by 0.5%–2% (Table S2) during June–October, and
528 the seasonal changes in rainfall and snowmelt contributions to total runoff closely mirror those
529 observed in the NX basin.
530
531 **4.2 Hydrological Response to Future Climate Changes**
532 Historical differences in total runoff changes in the NX and NX-BXK sub-basins are projected
533 to weaken in the future. The YZ basin is projected to experience increased precipitation (7–33
534 mm/10yr) and higher temperatures (0.3–0.8 °C/10yr) under the SSP2-4.5 and SSP5-8.5
535 scenarios throughout the 21st century (Table 5). Predictions indicate an increase in total runoff
536 for the NX (7–27 mm/10yr) and BXK (34–100 mm/10yr) for 2021–2100 under both SSPs,
537 with significant increases (36–142 mm/10yr) anticipated in the latter half of the century (2071–
538 2100) under SSP5-8.5 (Table 5). The changes in total runoff are projected to be primarily
539 influenced by increased rainfall runoff, with minor contributions from increased snowmelt and
540 glacier runoff under both SSPs scenario through the 21st century (Table 5). However, in
541 comparison to the 1971–2000 mean, a reduction of approximately -6% to -14% is projected in
542 the first half of the 21st century (2021–2050) in the YZ and its NX and NX-BXK sub-basins
543 under the SSP2-4.5 and SSP5-8.5 scenario (Figure 8). This reduction is attributed to decreased
544 rainfall (-9% to -19%) and snowmelt (-5% to -6%), which may result in the decline of

freshwater supply. Conversely, there is a broadly consistent increase (6%–32%) in total runoff in the second half of the 21st century (2071–2100), mainly driven by increased rainfall (4%–52%) and glacier runoff (9%–78%), suggesting that the YZ basin will not face a water supply crisis in the end of 21st century.

Changes in meltwater from glaciers and seasonal snow significantly impact total runoff, influencing both quantity and timing and are particularly important for water availability during warm and dry seasons (Barnett et al., 2005). Relative to the 1971–2000 mean, the future annual hydrograph appears relatively stable across all sub-basins (Figure 9), with 60%–80% of mean annual runoff occurring from June to September. However, a decline of about -18% to -3% is projected in each month during 2021–2050 under the two SSPs due to decreased monthly precipitation and precipitation-induced rainfall and snowmelt runoff (Table S3 and S4). In contrast, there is an anticipated increase of about 6%–40% in each month, particularly in summer (25%–40%), during 2071–2100 under the two SSPs. The increased total runoff in the NX basin is primarily attributed to increased rainfall runoff and spring snowmelt, indicating an earlier spring snow melt and delayed fall freeze-up (Figure 9a, b). Similarly, the increased total runoff in the NX-BXK basin is mostly a result of increased rainfall and glacier runoff, coupled with decreased snowmelt (Figure 9c, d), primarily due to reduced snowfall with ongoing warming in each month (Figure S4 and S5). Future changes in seasonal runoff across the entire YZ basin closely align with those in the NX-BXK sub-basin (Figure 9e, f) due to its significant

565 contribution to the overall runoff of the YZ basin.

566

567 **5 Discussion**

568 Forcing inputs, parameters, and representation of physical processes are major sources of
569 uncertainty in hydrological model simulations.

570

571 Precipitation is the most important atmospheric input for land surface hydrology models, but
572 none of the multiple precipitation datasets proves equally suitable for all basins in the TP due
573 to the high spatiotemporal variability in their performance at the sub-basin scale (Dahri et al.
574 2021). The variation in precipitation datasets for high mountains can lead to significant
575 differences in meltwater contribution (Lutz et al., 2014; Zhao et al., 2019; Sun and Su, 2020;
576 Khanal et al., 2021; Nan et al., 2021; Wang et al., 2021). Duethmann et al. (2014) applied a
577 multi-objective genetic algorithm to characterize the trade-off curve between model
578 performance in terms of discharge and snow cover area in Central Asia, suggesting that good
579 discharge simulations at the catchment outlet cannot guarantee good internal functioning of the
580 model, as different forcing inputs may result in error compensation among different runoff
581 compositions. Jost et al. (2012) simulated glacier runoff of 25 large glacierized basins
582 (>50,000 km^2) in North and South America, Europe, Asia, and New Zealand, suggesting that
583 the runoff differences ranged from 0.07 % for weakly glacier-influenced basins to 252 % for
584 strongly glacier-influenced basins. They also suggested that hydrologic model calibration in

585 glacier-fed catchments was difficult, because errors in modelling snow accumulation can be
586 offset by compensating errors in glacier melt. Zhang et al. (2013) simulated glacier runoff by
587 the VIC-Glacier model with the APHRODITE precipitation estimates in the upper Indus (UI)
588 river basin of the TP during 1961–2009, and suggeted that contribution of glacier runoff to total
589 runoff was about 48.2. However, Meng et al. (2023) simulated glacier runoff by the VIC-
590 Glacier model with the corrected MERRA-2 precipitation estimates in the UI basin, suggested
591 that glacier runoff contributed of 24% to total runoff. The difference between Zhang et al. (2013)
592 and Mengand (2023) mostly resulted from the higher amount of corrected MERRA-2 than
593 APHRODITE precipitation estimates in the UI basin, because the underestimation of
594 precipitation-induced runoff would be compensated by glacier runoff.
595
596 Like elsewhere on earth, the aforementioned issues are typical of the YZ basin. In the case of
597 the NX basin, glacier melt contributed approximately 2–18% to the total runoff in existing
598 research (Table 1), mostly resulting from differences in forcing inputs used in hydrological
599 models. The YZ basin received less attention regarding glacier runoff contributions in the NX-
600 BXK, with significant inconsistencies in glacier contributions evident in these studies (Table
601 1). Sun and Su (2020) suggested that mean annual glacier runoff contributed about 45% to total
602 runoff in the NX-BXK sub-basin for 1980–2000, using a hydrological model without
603 calibration and validation due to a lack of hydrometeorological observations in the sub-basin.
604 In this study, we utilized newly acquired rain gauge data, and streamflow, glacier mass balance,

and glacier and snow cover observations in the NX-BXK sub-basin, glacier runoff was simulated using the well-validated VIC-Glacier model, forced by a comprehensively reconstructed long-term precipitation dataset in this study. The updated contribution of glacier runoff to total runoff during 1971–2020 in the NX-BXK sub-basin was determined to be 19%. Furthermore, accurate historical precipitation estimates have the potential to reduce uncertainty in future projections with the large spread in the GCMs, forming the basis for correcting future GCM estimates. Different study period also results in the difference of hydrological model simulation. For example, streamflow also mutates in 1997 at the RKZ sub-basin of the YZ (Figure S15). Increased precipitation and evaporation caused an insignificant runoff change during 1971–1997. However, due to significant decrease of precipitation and increase of evaporation, runoff decreased during 1998–2000, resulting in the insignificant decrease for 1971–2000 (Figure S15).

Hydrological model themselves have their own uncertainties, such as model parameters and structure of physical processes, which are ideally all taken into account. Reliable parameters play a crucial role in accurate runoff simulation by hydrological models. The DDF emerges as the most sensitive parameter for the degree-day glacier model (Hock 2003; Radić; Hock 2010). Zhang et al. (2013) examined the sensitivity of glacier melt runoff to DDF parameters, suggesting that average annual glacier runoff could change by about 10% with each one unit

625 change in DDF (mm °C^{-1} day^{-1}). In this study, the DDF parameters are derived based on
626 observed glacier mass balance data, with intensive validations on glacier melt, including
627 observed glacier mass balance and satellite-based glacier area estimates. The uncertainty
628 associated with VIC model parameters is generally lower than the uncertainties from
629 precipitation inputs. Su et al. (2022) indicated that changes in the RB are within 8% when B_inf
630 ranges from 0.05 to 0.4, D2 ranges from 0.5 to 3.0 m, and the changes in NSE are generally
631 within 0.1. Therefore, high-density hydrometeorological observations are expected to better
632 constrain the model and further improve the description of hydrological responses to climate
633 and spatiotemporal changes in glacier/snow.
634
635 Uncertainties are introduced by different representation of physical processes in hydrological
636 model, especially the snow and glacier melt simulation in high-mountainous basins. Existing
637 studies used different definitions of runoff composition. For example, Lutz et al. (2014) and
638 Khanal et al. (2021) divided total runoff into four compositions: rainfall runoff, snow melt,
639 glacier melt and baseflow. Some studies also further divided the glacier melt into ice melt and
640 supraglacial snowmelt (Armstrong et al. 2018; Wang et al. 2021). In this study, we divided total
641 runoff into rainfall runoff, snow melt and glacier runoff. Baseflow is a relatively stable
642 streamflow composition, and it plays an important role in sustaining surface water flow,
643 especially for the winter half-year when surface water availability is limited. The VIC model
644 accounts for baseflow (https://vic.readthedocs.io/en/master/), which is comprised of three soil

layers to represent the rapid dynamics of soil moisture movement during storm events (surface runoff) and the slower deep inter-storm response in the bottom layer (baseflow). Figure S16 shows mean annual contribution and annual variation contribution of rainfall runoff, snowmelt, glacier runoff and baseflow to total runoff. The baseflow contribution was relatively stable, and it only contributed of 4% to total runoff in the NX basin since 1971. Wang et al. (2022) quantified the contribution of baseflow by the water and energy budget-based distributed hydrological model (WEB-DHM), and suggested mean annual baseflow contributed of 3.3% to total runoff. However, different model structures to represent baseflow processes may also result in uncertainties. In addition, the effect of climate change on the baseflow in the YZ basin remains uncertain mainly due to the generally poor understanding of mountain aquifers. Detailed study of infiltration and recharge processes, aquifer characteristics, and flow pathways needs to be a focus of future research to predict how baseflow will respond to the changes in climate and cryosphere.

The representation of glacier melting processes introduces substantial uncertainties in model simulations. The accuracy of distinguishing between debris-free and debris-covered glacier extents at the basin scale critically influences the simulated contribution of glacier runoff. Currently, the differentiation between these two glacier surface types relies on elevation constraints. However, due to the observation in these two glacier surface types, the DDFs were set to the same value in the debris-free and debris-covered glacier. To address this pivotal issue,

665 additional glacier observations encompassing both surface types, coupled with high-quality
666 remote sensing mapping, would solve this key issue. This approach holds the potential to refine
667 distinctions between debris-free and debris-covered glaciers, thereby enhancing the precision
668 of model simulations concerning glacier melting processes.
669
670 Another key issue is the restricted comprehension of the effect of snow and ice sublimation on
671 glacier runoff. Sublimation can potentially be an important component of the high-altitude
672 water balance in the Himalayan region (Lutz et al., 2016). Sublimation was mostly calculated
673 based on gauge measurement and estimated using an elevation-dependent potential sublimation
674 function (Lutz et al., 2016; Khanal et al., 2021; Stigter et al. 2018). Stigter et al. (2018)
675 suggested that the fraction of snowfall sublimation may be much higher than 21% at wind-
676 exposed locations in the Himalayan region. Lutz et al. (2016) and Khanal et al. (2021) proposed
677 that snow sublimation accounts for approximately 10% in the UI basin and 2%–3% in the YZ
678 basin. Furthermore, the impact of snow sublimation diminished as a result of a smaller fraction
679 of precipitation falling as snow with ongoing warming (Khanal et al., 2021). Yang et al. (2013)
680 investigated mass balance of a maritime glacier on the YZ basin of the southeast TP during
681 2005–2010, and indicated that the mass loss by way of sublimation/evaporation was quite
682 negligible (about -0.07 m/yr).
683
684 Runoff change is also influenced by land cover and land use. Liu et al. (2023) studied the effect

of vegetation growth induced by climate change to runoff variation during 1981–2010 in the YZ basin with the Variable Infiltration Capacity (VIC) model, suggesting that implanting grassland effectively reduces flash flood runoff in the short term and balances groundwater runoff in the long term. Broad-leaved and coniferous forests, with their longer growth cycles, also play a key role in adjusting soil moisture. Ji et al. (2023) explored the effect of vegetation growth on runoff changes in the YZ basin by computing the functional equation for the Normalized Difference Vegetation Index (NDVI) and Budyko parameter, suggesting that the NDVI and discharge both presented an increasing trend, and the contributions of NDVI on streamflow change in the 1998–2015 were about 43.04%.

6 Conclusions

This study comprehensively investigates runoff composition, flow changes, and their attribution across six sub-basins in the YZ for 1971–2020, with a particular focus on the comparison between the NX and NX-BXK using a newly generated precipitation dataset and a well-validated large-scale VIC-Glacier model with observed streamflow at eight hydrological stations, glacier mass balance data at two sites, and satellite-based glacier and snow cover estimates. The study also assesses the future evolution of annual and seasonal total water availability, as well as glacier runoff and snowmelt contributions, using an ensemble of multiple GCMs from CMIP6 under two SSPs. The key findings are summarized as follows:

1. Large regional differences in runoff regimes were observed in the YZ basin for 1971–2020. The NX-BXK contributed 52% to total runoff at the Pasighat outlet of the YZ basin, followed by the YC-NX (25%), LS (10%), and other sub-basins. While rain-induced runoff dominated the entire YZ (59%–72%), glacier runoff played a more important role in annual total runoff in downstream sub-basins (16%–19%), particularly in summer (23%–35%).

2. Regional differences in runoff changes were identified in the YZ basin. Annual runoff generally increased (8–19 mm/10yr) during 1971–2020 in all sub-basins of the NX basin, but a significant decrease is noted in the NX-BXK sub-basin (-9.4 mm/10yr). Total runoff trends reversed after 1998 for all sub-basins of the YZ, with increasing trends during 1971–1997 and decreasing trends during 1998–2020, influenced by changes in summer rainfall runoff due to atmospheric moisture and teleconnection indices (PDO, ENSO, and AMO). Glacier runoff mitigated the decreasing contribution from rainfall since 1998, exhibiting an increased effect on water supply.

3. Total runoff will consistently increase (27–100 mm/10yr) across the sub-basins through the 21st century, with increases of 7–27 mm/10yr in NX and 34–100 mm/10yr in NX-BXK under two SSPs, resulting from increased rainfall runoff and minor effect of increased snowmelt and glacier runoff. Relative to the 1971–2000 mean, a decrease of about -6% to -14% is expected

in the first half of the 21st century (2021–2050), followed by a consistent increase (6%–32%) in the second half (2071–2100).

Acknowledgments

This study was financially supported by the National Natural Science Foundation of China (42201140), a project funded by the China Postdoctoral Science Foundation (2022M723256), and the Second Tibetan Plateau Scientific Expedition and Research (STEP) Program (2019QZKK0201). We extend our gratitude to Daqing Yang, Ying Li, Qikai Sun and Tinghai Ou for their constructive suggestions.

Data availability

Daily precipitation, maximum and minimum temperature, and wind speed estimates with a spatial resolution of 10×10 km during 1971–2100 were adopted from Sun et al. (2022), and were downloaded from the National Tibetan Plateau/Third Pole Environment Data Center (TPDC, https://doi.org/10.11888/Atmos.tpdc.272885). Daily transient climate estimates, at a spatial resolution of 10×10 km for 1971–2100 under 20 scenarios (10 GCMs × 2 SSPs) used in this study were from Sun et al. (2024). Observed streamflow was from the Ministry of Water Resources, China. Two shapefiles of glacier inventory were downloaded from the "Environment & Ecological Science Data Center for west China" (http://westdc.westgis.ac.cn/glacier) and Randolph Glacier Inventory (RGI) 6.0

(https://www.glims.org/RGI/rgi60_dl.html). Observed annual glacier mass balance data from Gurenhekou and Parlung No.94 glacier sites since 2005 were downloaded from the TPDC. The snow cover fraction (SCF) estimates during 2006–2018 were form the Moderate Resolution Imaging Spectroradiometer (MODIS) 10CM (https://nsidc.org/ data).

Author Contributions

He Sun: Conceptualization, Formal analysis, Investigation, Methodology, Resources, Visualization, Funding acquisition, Writing draft. Tandong Yao: Writing (review and editing). Fengge Su: Writing (review and editing). Wei Yang: Editing and provision of glacier mass balance data. Deliang Chen: Writing (review and editing).

Competing interests

The authors declare that they have no known competing financial interests or personal relationships that could have appeared to influence the work reported in this paper.

References

An, B., Wang, W., Yang, W., Wu, G., Guo, Y., Zhu, H., et al.: Process, mechanisms, and early warning of glacier collapse-induced river blocking disasters in the Yarlung Tsangpo Grand Canyon, southeastern Tibetan Plateau, Sci. Total Environ., 151652, https://doi.org/10.1016/j.scitotenv.2021.151652, 2021.

766 Armstrong, R. L., Rittger, K., Brodzik, M. J., Racoviteanu, A., Barrett, A. P., Khalsa, S. J. S., et
767 al.: Runoff from glacier ice and seasonal snow in High Asia: separating melt water sources in
768 river flow, Reg. Environ. Change., 19, 1249-1261, https://doi.org/10.1007/s10113-018-1429-0,
769 2019.
770
771 Bahr, D. B., Meier, M. F., Peckham, S. D.: The physical basis of glacier volume-area scaling, J.
772 Geophys. Res. Solid Earth., 102, 20355-20362, https://doi.org/10.1029/97jb01696, 1997.
773
774 Barnett, T. P., Adam, J. C., Lettenmaier, D. P.: Potential impacts of a warming climate on water
775 availability in snow-dominated regions, Nature., 438, 303-309,
776 https://doi.org/10.1038/nature04141, 2005.
777
778 Chen, C., Zhang, L., Xiao, T., He, J.: Barrier lake bursting and flood routing in the Yarlung
779 Tsangpo Grand Canyon in October 2018, J. Hydrol., 583,
780 https://doi.org/10.1016/j.jhydrol.2020.124603, 2020.
781
782 Chen, X., Long, D., Hong, Y., Zeng, C., Yan, D.: Improved modeling of snow and glacier
783 melting by a progressive two-stage calibration strategy with GRACE and multisource data:
784 How snow and glacier meltwater contributes to the runoff of the Upper Brahmaputra River
785 basin?, Water Resour. Res., 53, 2431–2466, https://doi.org/10.1002/2016WR019656, 2017.

786

787 Cui, T., Li, Y., Yang, L., Nan, Y., Li, K., Tudaji, M., et al.: Non-monotonic changes in Asian
788 Water Towers' streamflow at increasing warming levels, Nat. Commun., 14(1), 1176,
789 https://doi.org/10.1038/s41467-023-36804-6, 2023.

790

791 Cuo, L., Zhang, Y.: Spatial patterns of wet season precipitation vertical gradients on the Tibetan
792 Plateau and the surroundings, Sci. Rep., 7, 5057, https://doi.org/10.1038/s41598-017-05345-6,
793 2017.

794

795 Cuo, L., Li, N., Liu, Z., Ding, J., Liang, L., Zhang, Y., Gong, T.: Warming and human activities
796 induced changes in the Yarlung Tsangpo basin of the Tibetan plateau and their influences on
797 streamflow, J. Hydrol. Reg. Stud., 25, 100625, https://doi.org/10.1016/j.ejrh.2019.100625,
798 2019.

799

800 Dahri, Z. H., Ludwig, F., Moors, E., Ahmad, S., Ahmad, B., Shoaib, M., et al.: Spatio‐temporal
801 evaluation of gridded precipitation products for the high‐altitude Indus basin, Int. J. Climatol.,
802 41, 4283-4306, https://doi.org/10.1002/joc.7073, 2021.

803

804 Duethmann, D., Peters, J., Blume, T., Vorogushyn, S., Güntner, A.: The value of satellite-
805 derived snow cover images for calibrating a hydrological model in snow-dominated catchments

806 in Central Asia, Water Resour. Res., 50, 2002-2021, https://doi.org/10.1002/2013WR014382,
807 2014.
808
809 Gao, C., Liu, L., Ma, D., He, K., Xu, Y. P.: Assessing responses of hydrological processes to
810 climate change over the southeastern Tibetan Plateau based on resampling of future climate
811 scenarios, Sci. Total Environ., 664, 737-752, https://doi.org/10.1016/j.scitotenv.2019.02.013,
812 2019.
813
814 Gu, H., Xu, Y. P., Liu, L., Xie, J., Wang, L., Pan, S., Guo, Y.: Seasonal catchment memory of
815 high mountain rivers in the Tibetan Plateau, Nat. Commun., 14(1), 3173,
816 https://doi.org/10.1038/s41467-023-38966-9, 2023.
817
818 Hoang, L. P., Lauri, H., Kummu, M., Koponen, J., van Vliet, M. T. H., Supit, I., Leemans, R.,
819 et al.: Mekong River flow and hydrological extremes under climate change, Hydrol. Earth Syst.
820 Sci., 20, 3027-3041, https://doi.org/10.5194/hess-20-3027-2016, 2016.
821
822 Hock, R.: Temperature index melt modelling in mountain areas, J. Hydrol., 282, 104-115,
823 https://doi.org/10.1016/s0022-1694(03)00257-9, 2003.
824
825 Ji, G., Yue, S., Zhang, J., Huang, J., Guo, Y., Chen, W.: Assessing the impact of vegetation

826 variation, climate and human factors on the streamflow variation of Yarlung Zangbo river with
827 the corrected Budyko equation, Forests, 14(7), 1312, https://doi.org/10.3390/f14071312, 2023.
828
829 Jost, G., Moore, R. D., Menounos, B., Wheate, R.: Quantifying the contribution of glacier
830 runoff to streamflow in the upper Columbia River Basin, Canada, Hydrol. Earth Syst. Sci., 16,
831 849-860, https://doi.org/10.5194/hess-16-849-2012, 2012.
832
833 Kan, B., Su, F., Xu, B., Xie, Y., Li, J., Zhang, H.: Generation of High Mountain Precipitation
834 and Temperature Data for a Quantitative Assessment of Flow Regime in the Upper Yarkant
835 Basin in the Karakoram, J. Geophys. Res. Atmos., 123, 8462-8486,
836 https://doi.org/10.1029/2017jd028055, 2018.
837
838 Khanal, S., Lutz, A. F., Kraaijenbrink, P. D., van den Hurk, B., Yao, T., Immerzeel, W. W.:
839 Variable 21st-century climate change response for rivers in High Mountain Asia at seasonal to
840 decadal time scales, Water Resour. Res., e2020WR029266,
841 https://doi.org/10.1029/2020WR029266, 2021.
842
843 Li, C., Su, F., Yang, D., Tong, K., Meng, F., Kan, B.: Spatiotemporal variation of snow cover
844 over the Tibetan Plateau based on MODIS snow product, 2001-2014, Int. J. Climatol., 38, 708-
845 728, https://doi.org/10.1002/joc.5204, 2018.

Liang, X., Lettenmaie, D. P., Wood, E. F., Burges, S. J.: A simple hydrologically based model of land-surface water and energy fluxes, J. Geophys. Res. Atmos., 99, 14415–14428, https://doi.org/10.1029/94jd00483, 1994.

Liang, X., Lettenmaier, D. P., Wood, E. F.: One-dimensional statistical dynamic representation of subgrid spatial variability of precipitation in the two-layer variable infiltration capacity model, J. Geophys. Res. Atmos., 101, 21403-21422, https://doi.org/10.1029/96jd01448, 1996.

Liu, L., Gu, H., Xie, J., Xu, Y. P.: How well do the ERA‐Interim, ERA‐5, GLDAS‐2.1 and NCEP‐R2 reanalysis datasets represent daily air temperature over the Tibetan Plateau?, Int. J. Climatol., 41, 1484-1505, https://doi.org/10.1002/joc.6867, 2020.

Liu, L., Pan, S. L., Bai, Z. X., Xu, Y. P.: Potential application of hydrological ensemble prediction in forecasting flood and its components over the Yarlung Zangbo River Basin, China, Hydrol. Earth Syst. Sci. Discuss., 1-33, https://doi.org/10.5194/hess-2018-179, 2018.

Liu, S., Sun, W., Shen, Y., Li, G.: Glacier changes since the Little Ice Age maximum in the western Qilian Shan, northwest China, and consequences of glacier runoff for water supply, J. Glaciol., 49, 117-124, https://doi.org/10.3189/172756503781830926, 2003.

866

867 Liu, X., Lu, H., Yang, K., Xu, Z., Wang, J.: Responses of runoff processes to vegetation
868 dynamics during 1981–2010 in the Yarlung Zangbo River basin, J. Hydrol. Reg. Stud., 50,
869 101553, https://doi.org/10.1016/j.ejrh.2021.100845, 2023.

870

871 Liu, Y., Wu, G., Hong, J., Dong, B., Duan, A., Bao, Q., Zhou, L.: Revisiting Asian monsoon
872 formation and change associated with Tibetan Plateau forcing: II. Chang, Clim. Dynam., 39,
873 1183-1195, https://doi.org/10.1007/s00382-012-1335-y, 2012.

874

875 Lutz, A. F., Immerzeel, W. W., Kraaijenbrink, P. D., Shrestha, A. B., Bierkens, M. F.: Climate
876 Change Impacts on the Upper Indus Hydrology: Sources, Shifts and Extremes, PLoS One, 11,
877 e0165630, https://doi.org/10.1371/journal.pone.0165630, 2016.

878

879 Lutz, A. F., Immerzeel, W. W., Shrestha, A. B., Bierkens, M. F. P.: Consistent increase in High
880 Asia's runoff due to increasing glacier melt and precipitation, Nat. Clim. Change., 4, 587-592,
881 https://doi.org/10.1038/nclimate2237, 2014.

882

883 Meng, F. C., Su, F. G., Li, Y., Tong, K.: Changes in Terrestrial Water Storage During 2003-2014
884 and Possible Causes in Tibetan Plateau, J. Geophys. Res. Atmos., 124, 2909-2931,
885 https://doi.org/10.1029/2018jd029552, 2019.

886

887 Meng, F., Su, F., Sun, H., Huang, J., Li, C.: Divergent runoff regime revealed by hydrological
888 simulations with corrected precipitation in the upper Indus, J. Hydrol., 626, 130315,
889 https://doi.org/10.1016/j.jhydrol.2023.130315, 2023.

890

891 Miao, L., Li, S., Zhang, F., Chen, T., Shan, Y., Zhang, Y.: Future Drought in the Dry Lands of
892 Asia Under the 1.5 and 2.0 °C Warming Scenarios, Earth's Future, 8, e2019EF001337,
893 https://doi.org/10.1029/2019ef001337, 2020.

894

895 Nan, Y., Tian, L., He, Z., Tian, F., Shao, L.: The value of water isotope data on improving
896 process understanding in a glacierized catchment on the Tibetan Plateau, Hydrol. Earth Syst.
897 Sci., 25(6), 3653-3673, https://doi.org/10.5194/hess-25-3653-2021, 2021.

898

899 Niu, Q., Liu, L., Heng, J., Li, H., Xu, Z.: A Multi-Index Evaluation of Drought Characteristics
900 in the Yarlung Zangbo River Basin of Tibetan Plateau, Southwest China, Front. Earth Sci., 8,
901 213, https://doi.org/10.3389/feart.2020.00213, 2020.

902

903 Pradhan, N. S., Das, P. J., Gupta, N., Shrestha, A. B.: Sustainable Management Options for
904 Healthy Rivers in South Asia: The Case of Brahmaputra, Sustainability, 13, 1987,
905 https://doi.org/10.3390/su13031087, 2021.

Pritchard, H. D.: Asia's shrinking glaciers protect large populations from drought stress, Nature, 569, 649-654, https://doi.org/10.1038/s41586-019-1240-1, 2019.

Qi, W., Liu, J., Chen, D.: Evaluations and Improvements of GLDAS2.0 and GLDAS2.1 Forcing Data's Applicability for Basin Scale Hydrological Simulations in the Tibetan Plateau, J. Geophys. Res. Atmos., 123, 13,128-113,148, https://doi.org/10.1029/2018JD029116, 2018.

Radić, V., Hock, R.: Regional and global volumes of glaciers derived from statistical upscaling of glacier inventory data, J. Geophys. Res. Earth, 115, https://doi.org/10.1029/2009JF001373, 2010.

Shi, X. G., Wood, A. W., Lettenmaier, D. P.: How Essential is Hydrologic Model Calibration to Seasonal Streamflow Forecasting?, J. Hydrometeorol., 9(6), 1350–1363, https://doi.org/10.1175/2008JHM1001.1, 2008.

Stigter, E. E., Litt, M., Steiner, J. F., Bonekamp, P. N. J., Shea, J. M., Bierkens, M. F. P., et al.: The Importance of Snow Sublimation on a Himalayan Glacier, Front. Earth Sci., 6, 108, https://doi.org/10.3389/feart.2018.00108, 2018.

926 Su, F., Hong, Y., Lettenmaier, D. P.: Evaluation of TRMM Multisatellite Precipitation Analysis
927 (TMPA) and Its Utility in Hydrologic Prediction in the La Plata Basin, J. Hydrometeorol., 9,
928 622-640, https://doi.org/10.1175/2007jhm944.1, 2008.
929
930 Su, F., Pritchard, H. D., Yao, T., Huang, J., Ou, T., Meng, F., et al.: Contrasting Fate of Western
931 Third Pole's Water Resources Under 21st Century Climate Change, Earth's Future, 10,
932 https://doi.org/10.1029/2022ef002776, 2022.
933
934 Su, F., Zhang, L., Ou, T., Chen, D., Yao, T., Tong, K., et al.: Hydrological response to future
935 climate changes for the major upstream river basins in the Tibetan Plateau, Glob. Planet. Chang.,
936 136, 82-95, https://doi.org/10.1016/j.gloplacha.2015.10.012, 2016.
937
938 Sun, H., Su, F.: Precipitation correction and reconstruction for streamflow simulation based on
939 262 rain gauges in the upper Brahmaputra of southern Tibetan Plateau, J. Hydrol., 590,
940 https://doi.org/10.1016/j.jhydrol.2020.125484, 2020.
941
942 Sun, H., Su, F., He, Z., Ou, T., Chen, D., Li, Z., et al.: Hydrological evaluation of high-resolution
943 precipitation estimates from the WRF model in the Third Pole river basins, J. Hydrometeorol.,
944 https://doi.org/10.1175/jhm-d-20-0272.1, 2021.
945

946 Sun, H., Yao, T., Su, F., He, Z., Tang, G., Li, N., et al.: Corrected ERA5 precipitation by machine
947 learning significantly improved flow simulations for the Third Pole basins, J. Hydrometeorol.,
948 23, https://doi.org/10.1175/JHM-D-22-0015.1, 2022.
949
950 Sun, H., Yao, T., Su, F., Ou, T., He, Z., Tang, G., et al.: Increased glacier melt enhances future
951 extreme floods in the southern Tibetan Plateau, Adv. Clim. Change Res., 2024.
952
953 Tang, Q., Lan, C., Su, F., Liu, X., Sun, H., Ding, J., et al.: Streamflow change on the Qinghai-
954 Tibet Plateau and its impacts, Chin. Sci. Bull., 64(27), 2807–2821, https://doi.org/10.1360/TB-
955 2019-0141, 2019.
956
957 Tong, K., Su, F., Xu, B.: Quantifying the contribution of glacier meltwater in the expansion of
958 the largest lake in Tibet, J. Geophys. Res. Atmos., 121, 11158–11173,
959 https://doi.org/10.1002/2016jd025424, 2016.
960
961 Tong, K., Su, F., Yang, D., Zhang, L., Hao, Z.: Tibetan Plateau precipitation as depicted by
962 gauge observations, reanalyses and satellite retrievals, Int. J. Climatol., 34, 265-285,
963 https://doi.org/10.1002/joc.3682, 2014.
964
965 Wang, A., Zeng, X.: Evaluation of multireanalysis products with in situ observations over the

966 Tibetan Plateau, J. Geophys. Res. Atmos., 117(D5), https://doi.org/10.1029/2011jd016553,
967 2012.
968
969 Wang, A., Wang, Y., Su, B., Kundzewicz, Z. W., Tao, H., Wen, S., et al.: Comparison of
970 Changing Population Exposure to Droughts in River Basins of the Tarim and the Indus, Earth's
971 Future, 8, https://doi.org/10.1029/2019ef001448, 2020.
972
973 Wang, L., Cuo, L., Luo, D., Su, F., Ye, Q., Yao, T., et al.: Observing multi-sphere hydrological
974 changes in the largest river basin of the Tibetan Plateau, Bull. Am. Meteorol. Soc., 103(6),
975 E1595-E1620, https://doi.org/10.1175/BAMS-D-21-0217.1, 2022.
976
977 Wang, X., Luo, Y., Sun, L., Shafeeque, M.: Different climate factors contributing for runoff
978 increases in the high glacierized tributaries of Tarim River Basin, China, J. Hydrol. Reg. Stud.,
979 36, 100845, https://doi.org/10.1016/j.ejrh.2021.100845, 2021.
980
981 Wang, Y., Wang, L., Zhou, J., Yao, T., Yang, W., Zhong, X., et al.: Vanishing glaciers at southeast
982 Tibetan Plateau have not offset the declining runoff at Yarlung Zangbo, Geophys. Res. Lett., 48,
983 e2021GL094651, https://doi.org/10.1029/2021gl094651, 2021.
984
985 Wu, G., Duan, A.: Weakening Trend in the Atmospheric Heat Source over the Tibetan Plateau

986 during Recent Decades. Part I: Observations, J. Clim., 21, 3149-3164,
987 https://doi.org/10.1175/2007jcli1912.1, 2008.
988
989 Wood, A. W.: Long-range experimental hydrologic forecasting for the eastern United States, J.
990 Geophys. Res. Atmos., 107(D20), ACL-6, https://doi.org/1029/2001JD000659, 2002.
991
992 Wood, A. W., Leung, L. R., Sridhar, V., Lettenmaier, D. P.: Hydrologic Implications of
993 Dynamical and Statistical Approaches to Downscaling Climate Model Outputs, Clim. Change.,
994 62, 189-216, https://doi.org/10.1023/B:CLIM.0000013685.99609.9e, 2004.
995
996 Wu, G., Duan, A.: Weakening Trend in the Atmospheric Heat Source over the Tibetan Plateau
997 during Recent Decades. Part II: Connection with Climate Warming, J. Clim., 22, 4197-4212,
998 https://doi.org/10.1175/2009jcli2699.1, 2009.
999
1000 Yang, W., Guo, X., Yao, T., Yang, K., Zhao, L., Li, S., et al.: Summertime surface energy budget
1001 and ablation modeling in the ablation zone of a maritime Tibetan glacier, J. Geophys. Res.
1002 Atmos., 116, https://doi.org/10.1029/2010jd015183, 2011.
1003
1004 Yang, W., Yao, T., Guo, X., Zhu, M., Li, S., Kattel, D. B.: Mass balance of a maritime glacier
1005 on the southeast Tibetan Plateau and its climatic sensitivity, J. Geophys. Res. Atmos., 118, 9579-

9594, https://doi.org/10.1002/jgrd.50760, 2013.

Yang, Y., Gao, D., Li, B.: Study on the moisture passage on the lower reaches of the Yarlung Zangbo river, Sci. China (Ser. B), 32, 580-593, 1989.

Yang, Z., Zhuo, M., Lu, H., Ma, P., Zhou, K.: Characteristics of precipitation variation and its effects on runoff in the Yarlung Zangbo River basin during 1961–2010, J. Glaciol. Geocryol., 36, 166-172, 2014 (in Chinese).

Yao, T., Bolch, T., Chen, D., Gao, J., Immerzeel, W., Piao, S., et al.: The imbalance of the Asian water tower, Nat. Rev. Earth Environ., 3(10), 618-632, https://doi.org/s43017-022-00299-4, 2022.

Yao, T., Thompson, L., Yang, W., Yu, W., Gao, Y., Guo, X., et al.: Different glacier status with atmospheric circulations in Tibetan Plateau and surroundings, Nat. Clim. Chang., 2, 663-667, https://doi.org/10.1038/nclimate1580, 2012.

Yao, T.: Recent glacial retreat in High Asia in China and its impact on water resource in Northwest China, Sci. China (Ser. D), 47, 1065, https://doi.org/10.1360/03yd0256, 2004.

1026 Zhang, L., Su, F., Yang, D., Hao, Z., Tong, K.: Discharge regime and simulation for the
1027 upstream of major rivers over Tibetan Plateau, J. Geophys. Res. Atmos., 118, 8500-8518,
1028 https://doi.org/10.1002/jgrd.50665, 2013.
1029
1030 Zhao, C., Yang, W., Westoby, M., An, B., Wu, G., Wang, W., et al.: Brief communication: An
1031 approximately 50 Mm ice-rock avalanche on 22 March 2021 in the Sedongpu valley,
1032 southeastern Tibetan Plateau, The Cryosphere, 16, 1333-1340, https://doi.org/10.5194/tc-16-
1033 1333-2022, 2022.
1034
1035 Zhao, Q., Ding, Y., Wang, J., Gao, H., Zhang, S., Zhao, C., et al.: Projecting climate change
1036 impacts on hydrological processes on the Tibetan Plateau with model calibration against the
1037 Glacier Inventory Data and observed streamflow, J. Hydrol., 573, 60-81,
1038 https://doi.org/10.1016/j.jhydrol.2019.03.043, 2019.
1039
1040 Zhong, L., Ma, Y., Fu, Y., Pan, X., Hu, W., Su, Z., et al.: Assessment of soil water deficit for the
1041 middle reaches of Yarlung-Zangbo River from optical and passive microwave images, Remote
1042 Sens. Environ., 142, 1-8, https://doi.org/10.1016/j.rse.2013.11.008, 2014.

Captions:

Figure 1. (a) Location and topography of the Yarlung Zangbo (YZ) river basin. Sub-basins, numbered 1 to 6, represent Lhatse (LZ), Lhatse-Yangcun (LZ-YC), Shigatse (RKZ), Lhasa (LS), Yangcun-Nuxia (YC-NX), and Nuxia-Pasighat (NX-BXK), respectively. (b) Spatial pattern of average annual streamflow for 1971–2020 in the YZ basin. The lower histogram shows the mean annual streamflow contribution from each sub-basin to the Pasighat outlet for 1971–2020 in the YZ..... 39

Figure 2. Mean monthly simulated rainfall, snowmelt, and glacier runoff, along with their contribution to total annual runoff in the YZ and its sub-basins for 1971–2020. 40

Figure 3. Spatial pattern of average annual rainfall runoff (a), snowmelt (c), glacier runoff (e), and precipitation (b) for 1971–2020 in the YZ basin. The spatial pattern of average annual snow cover fraction (SCF, d) for 2001–2019 and glacier distribution in the YZ basin. Percentage (%) of three runoff components (rainfall, snowmelt, and glacier runoff) at four elevation bands in the YZ basin, with the number in parentheses indicating the number of 10-km grids in each elevation band. 41

Figure 4. Annual trends in precipitation (mm/10yr), temperature (°C/10yr), total runoff (mm/10yr), and three runoff components (rainfall, glacier, and snowmelt runoff, mm/10yr) in the six sub-basins for 1971–2020, respectively. Asterisks indicate the 95% significance level. 37

Figure 5. Mean monthly vertical integral of atmospheric moisture budget (mm) in June, July, August, and September from the ERA5 data across the Yarlung Zangbo river basin for 1971–2020 (indicated by colors). Arrows represent the directions of the vertical integral of water vapor flux ($kg \cdot m^{-1} \cdot s^{-1}$)..... 38

Figure 6. Seasonal trends in precipitation (mm/10yr), temperature (°C/10yr), total runoff (mm/10yr), and three runoff components (rainfall, glacier, and snowmelt runoff, mm/10yr) in the YZ and its sub-basins for 1971–2020, respectively. 39

Figure 7. Changes in (a–c) mean monthly total runoff, (d–f) three components, and (g–i) their contributions to

total runoff for the period 1998–2020 relative to the period 1971–1997 in the entire YZ basin and its NX and NX-BXK sub-basins. 40

Figure 8. Projected changes (%) in the mean annual total runoff, and three runoff components (rainfall, glacier, and snowmelt) in 2021–2050 and 2071–2100, respectively, relative to 1971–2000 under the two SSPs in the YZ and its NX and NX-BXK sub-basins. 41

Figure 9. Monthly average of total runoff (mm) in 1971–2000, 2021–2050, and 2071–2100 and the change (mm) in their runoff components relative to 1971–2000. Dotted solid lines represent simulated mean monthly total runoff in three periods. Bar plots indicate the mean seasonal changes in rainfall, snowmelt, and glacier runoff in 2021–2050 and 2071–2100 relative to 1971–2000, based on the ensemble means of 10 hydrological simulations under the two SSPs in the YZ and its NX and NX-BXK sub-basins. 42

Table 1. Summary of relevant studies on simulated runoff component contributions in the YZ basin. 43

Table 2. Characteristics of the six sub-basins in the Yarlung Zangbo River 44

Table 3. Values of the first (D1, m), the second soil depth (D2, m) and degree-day factor (DDF), and the Nash-Sutcliffe Efficiency (NSE) and Relative Bias (RB, %) of the simulated monthly streamflow with the Variable Infiltration Capacity (VIC)-Glacier model relative to the observation for the eight hydrological stations. 45

Table 4. Trends in precipitation, temperature, total runoff, and three runoff components and their contributions to total runoff in the YZ and its NX and NX-BXK sub-basins for different periods. Asterisks indicate the 95% confidence level. 46

Table 5. Trends of projected annual precipitation (mm/10 yr), temperature (°C/10 yr), and total runoff and runoff components (mm per decade) from 10 GCMs for 1971–2000, 2021–2050, and 2071–2100 under the two SSPs in the YZ and its two sub-basins (The uncertainties are indicated with one standard deviation). 47

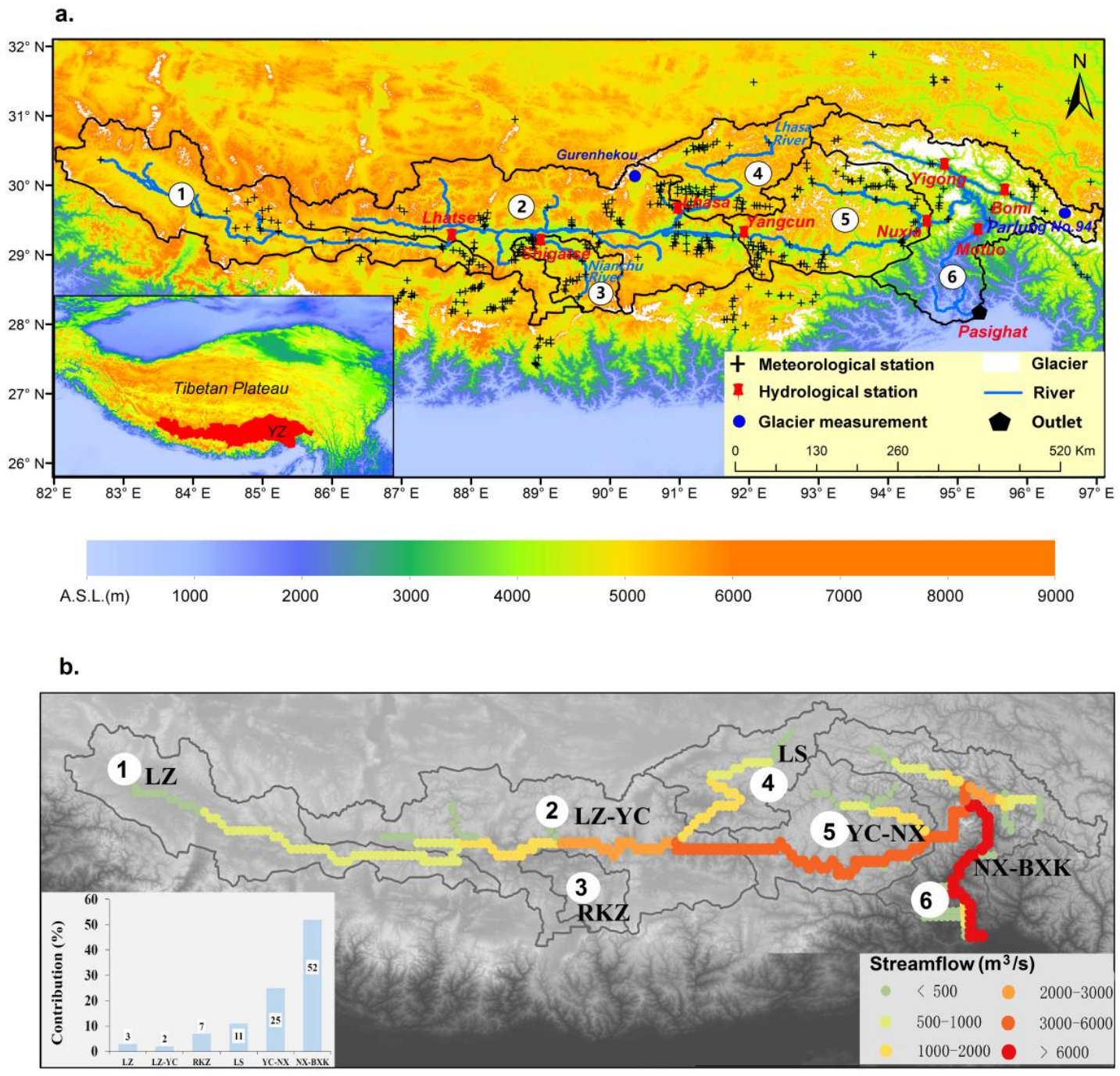

Figure 1. (a) Location and topography of the Yarlung Zangbo (YZ) river basin. Sub-basins, numbered 1 to 6, represent Lhatse (LZ), Lhatse-Yangcun (LZ-YC), Shigatse (RKZ), Lhasa (LS), Yangcun-Nuxia (YC-NX), and Nuxia-Pasighat (NX-BXK), respectively. (b) Spatial pattern of average annual streamflow for 1971–2020 in the YZ basin. The lower histogram shows the mean annual streamflow contribution from each sub-basin to the Pasighat outlet for 1971–2020 in the YZ.

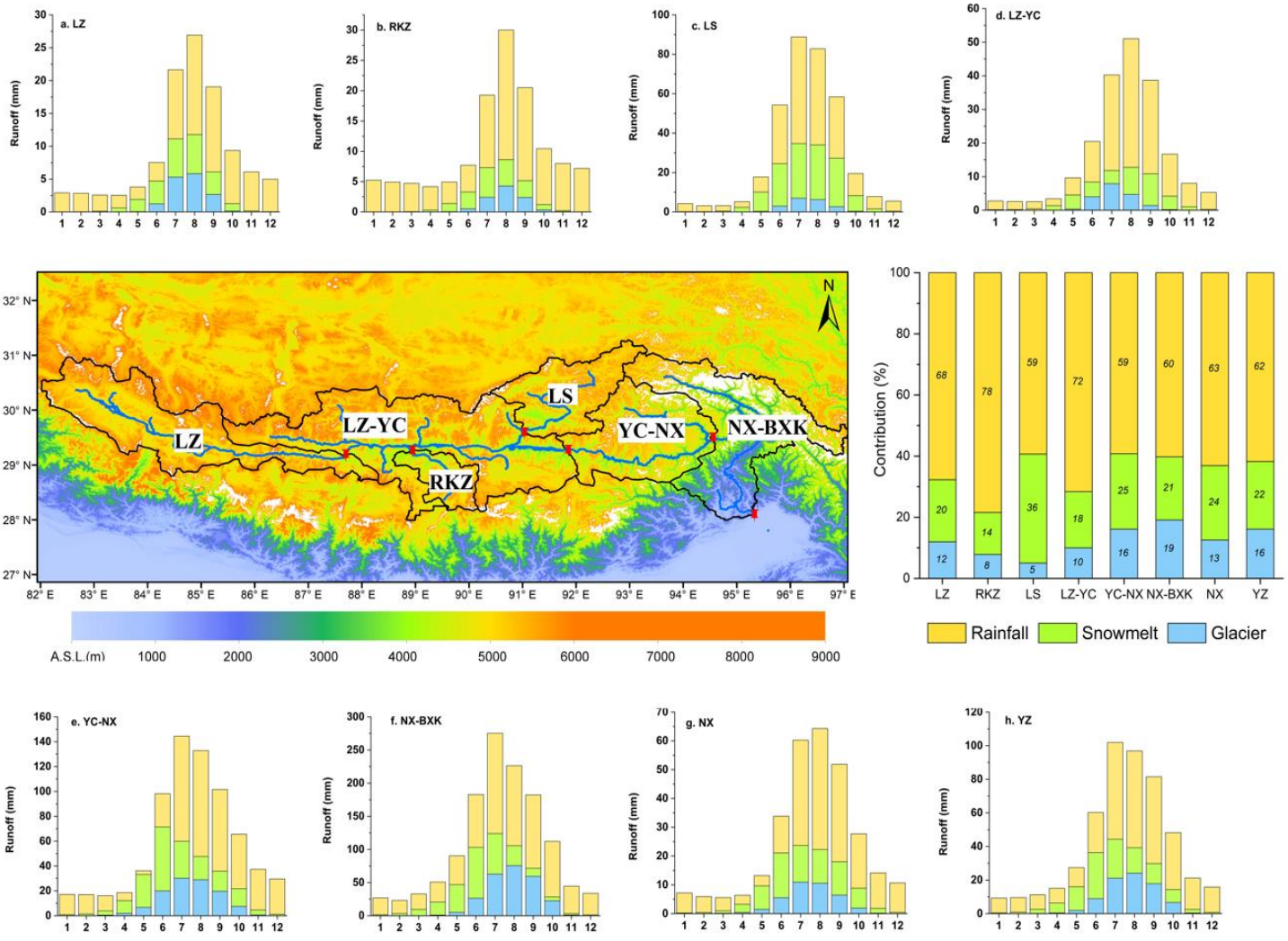

Figure 2. Mean monthly simulated rainfall, snowmelt, and glacier runoff, along with their contribution to total annual runoff in the YZ and its sub-basins for 1971–2020.

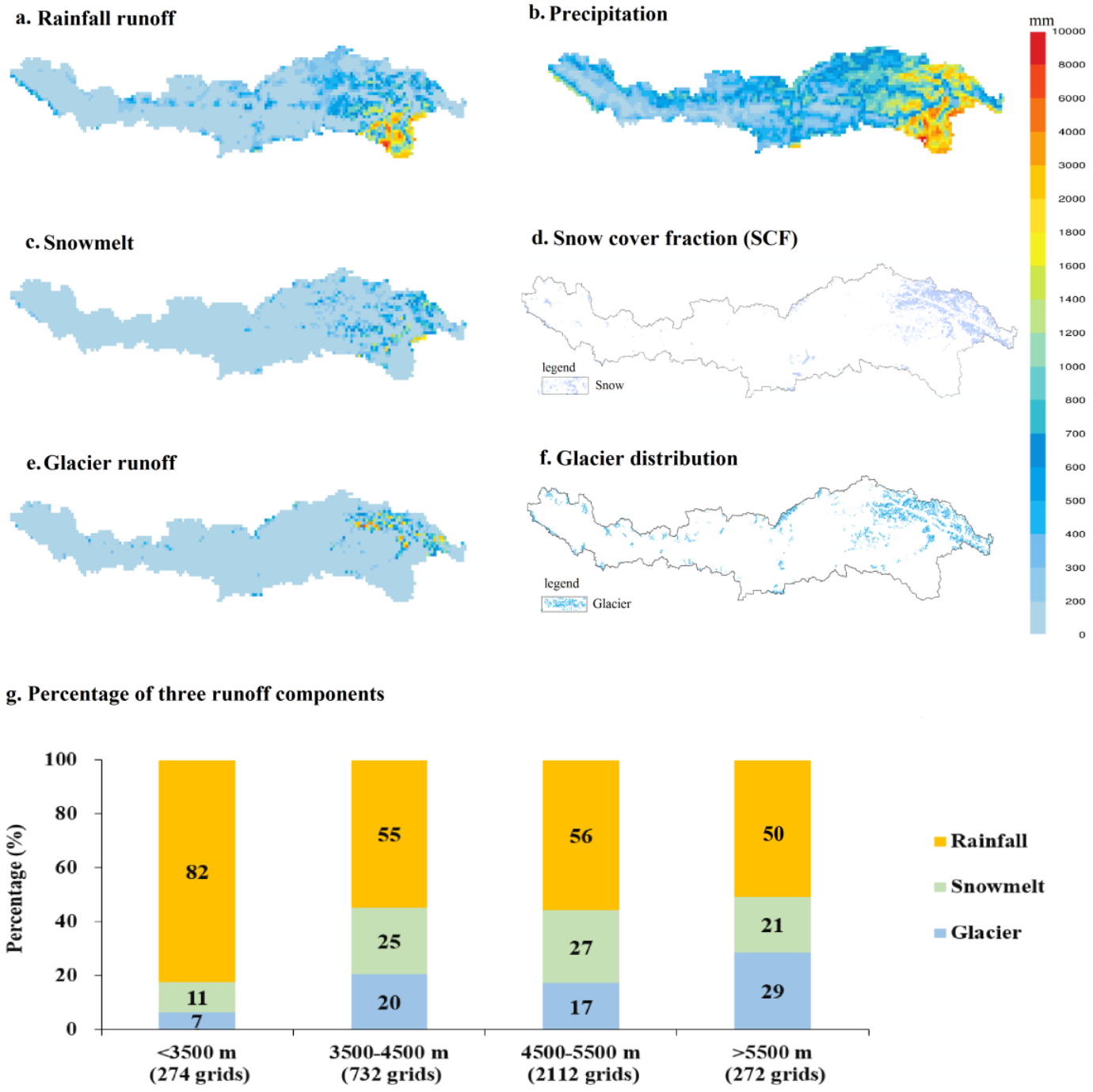

Figure 3. Spatial pattern of average annual rainfall runoff (a), snowmelt (c), glacier runoff (e), and precipitation (b) for 1971–2020 in the YZ basin. The spatial pattern of average annual snow cover fraction (SCF, d) for 2001–2019 and glacier distribution in the YZ basin. Percentage (%) of three runoff components (rainfall, snowmelt, and glacier runoff) at four elevation bands in the YZ basin, with the number in parentheses indicating the number of 10-km grids in each elevation band.

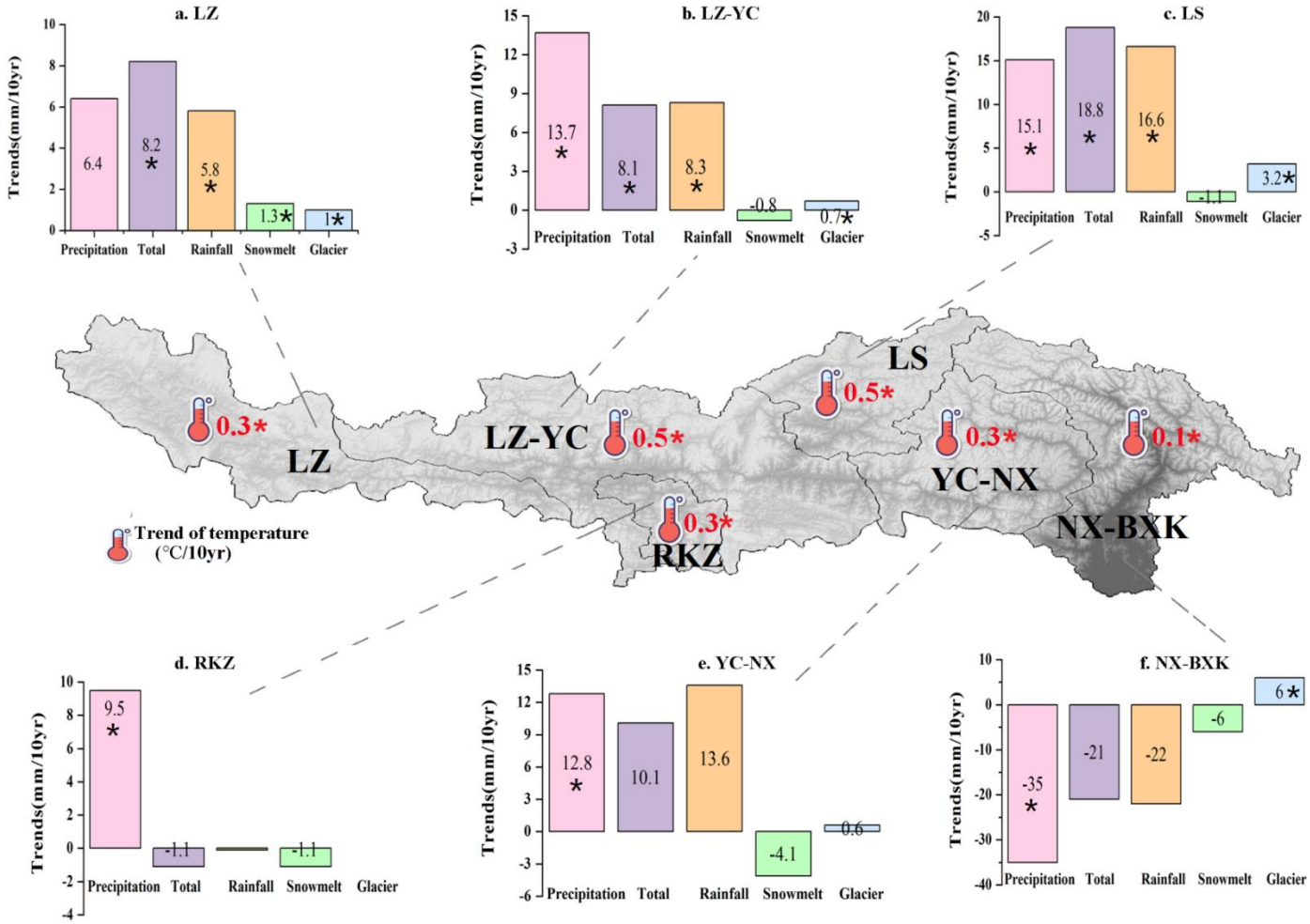

Figure 4. Annual trends in precipitation (mm/10yr), temperature (°C/10yr), total runoff (mm/10yr), and three runoff components (rainfall, glacier, and snowmelt runoff, mm/10yr) in the six sub-basins for 1971–2020, respectively. Asterisks indicate the 95% significance level.

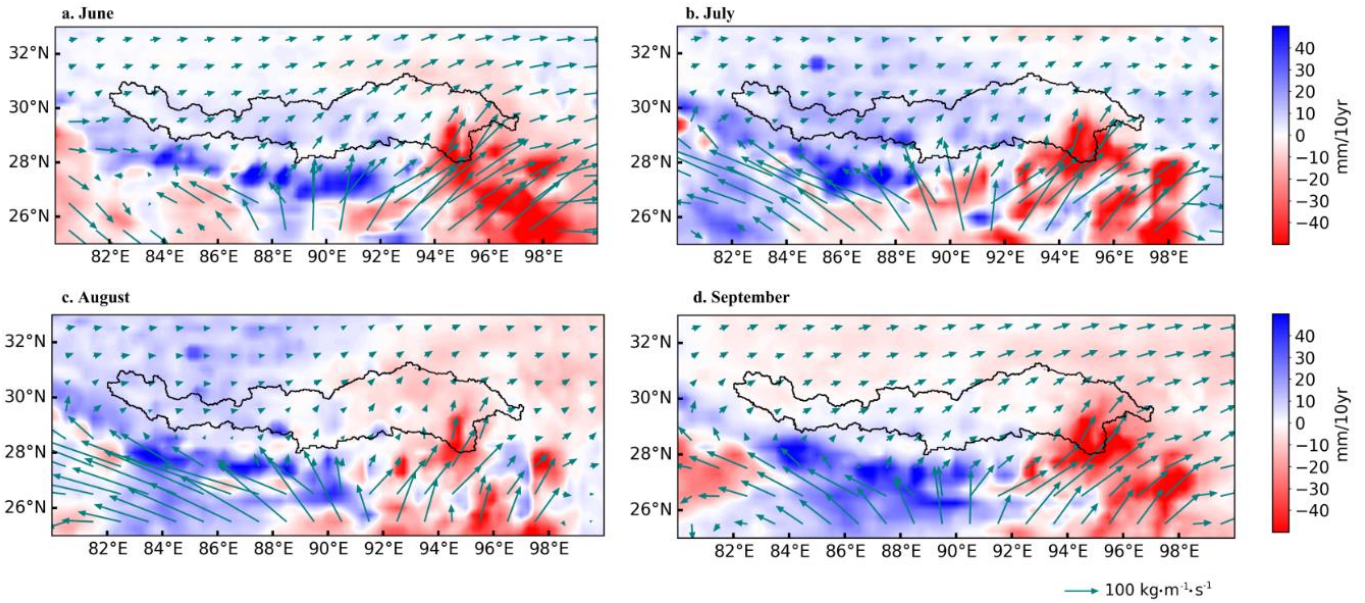

Figure 5. Mean monthly vertical integral of atmospheric moisture budget (mm) in June, July, August, and September from the ERA5 data across the Yarlung Zangbo river basin for 1971–2020 (indicated by colors). Arrows represent the directions of the vertical integral of water vapor flux ($kg \cdot m^{-1} \cdot s^{-1}$).

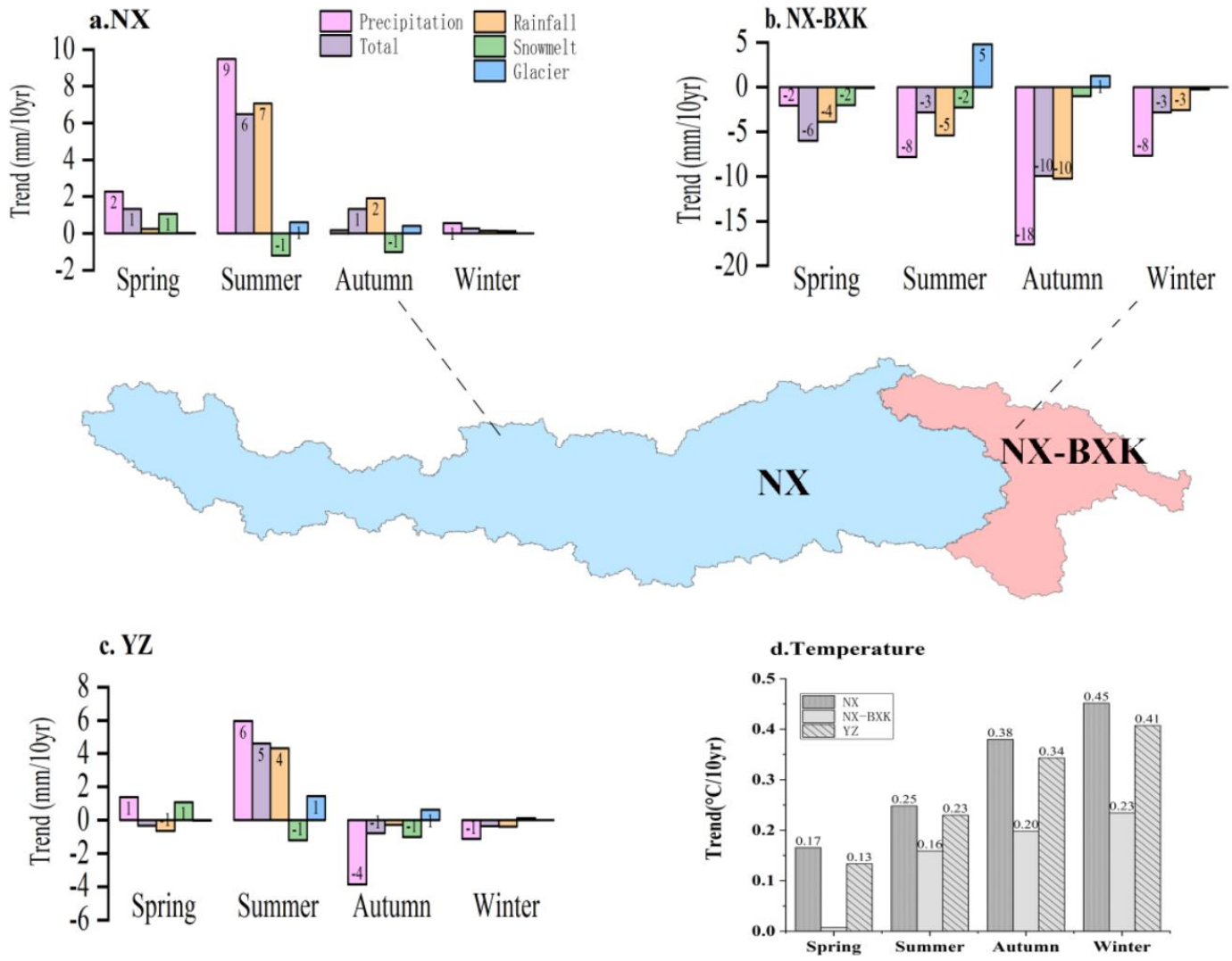

Figure 6. Seasonal trends in precipitation (mm/10yr), temperature (°C/10yr), total runoff (mm/10yr), and three runoff components (rainfall, glacier, and snowmelt runoff, mm/10yr) in the YZ and its sub-basins for 1971–2020, respectively.

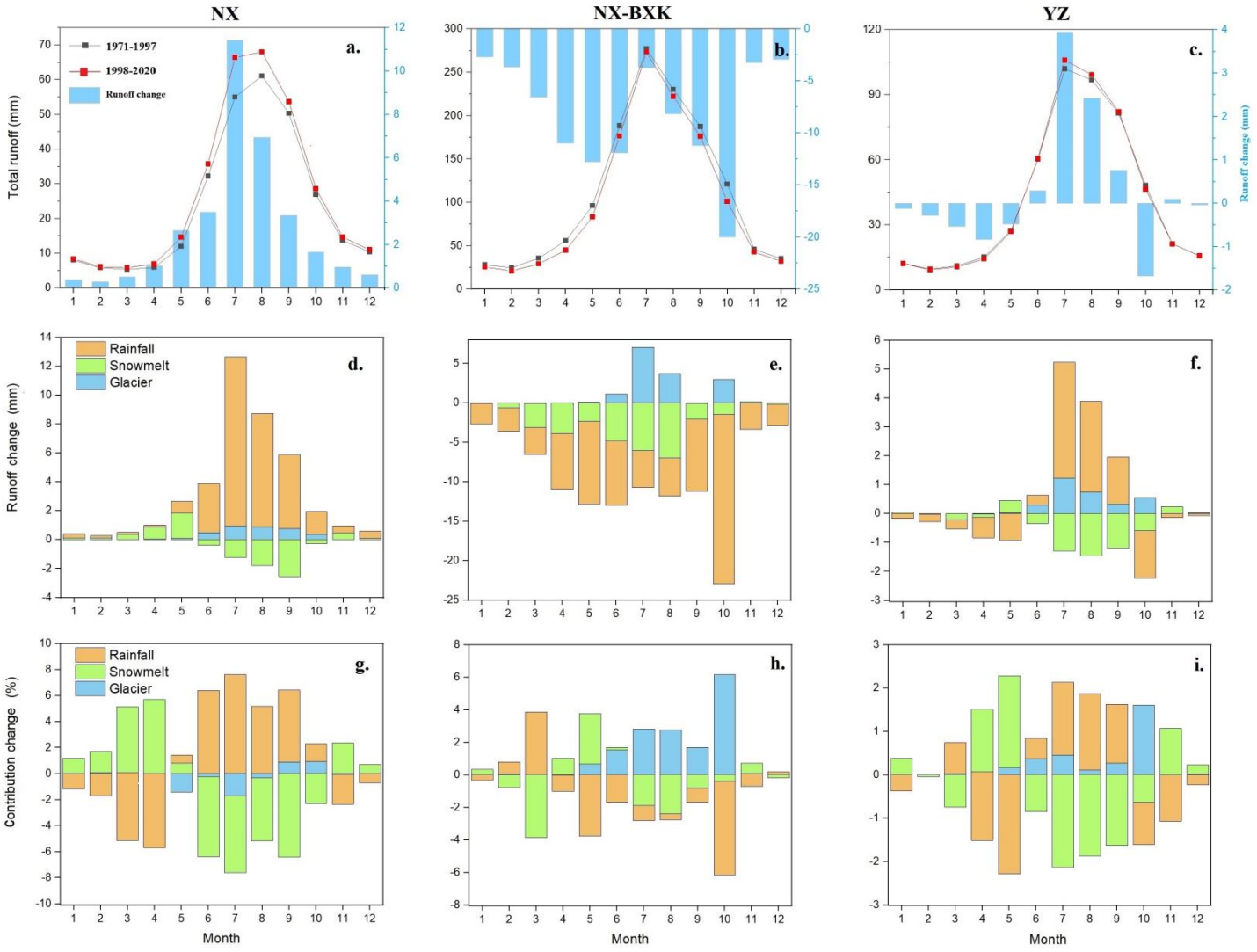

Figure 7. Changes in (a–c) mean monthly total runoff, (d–f) three components, and (g–i) their contributions to total runoff for the period 1998–2020 relative to the period 1971–1997 in the entire YZ basin and its NX and NX-BXK sub-basins.

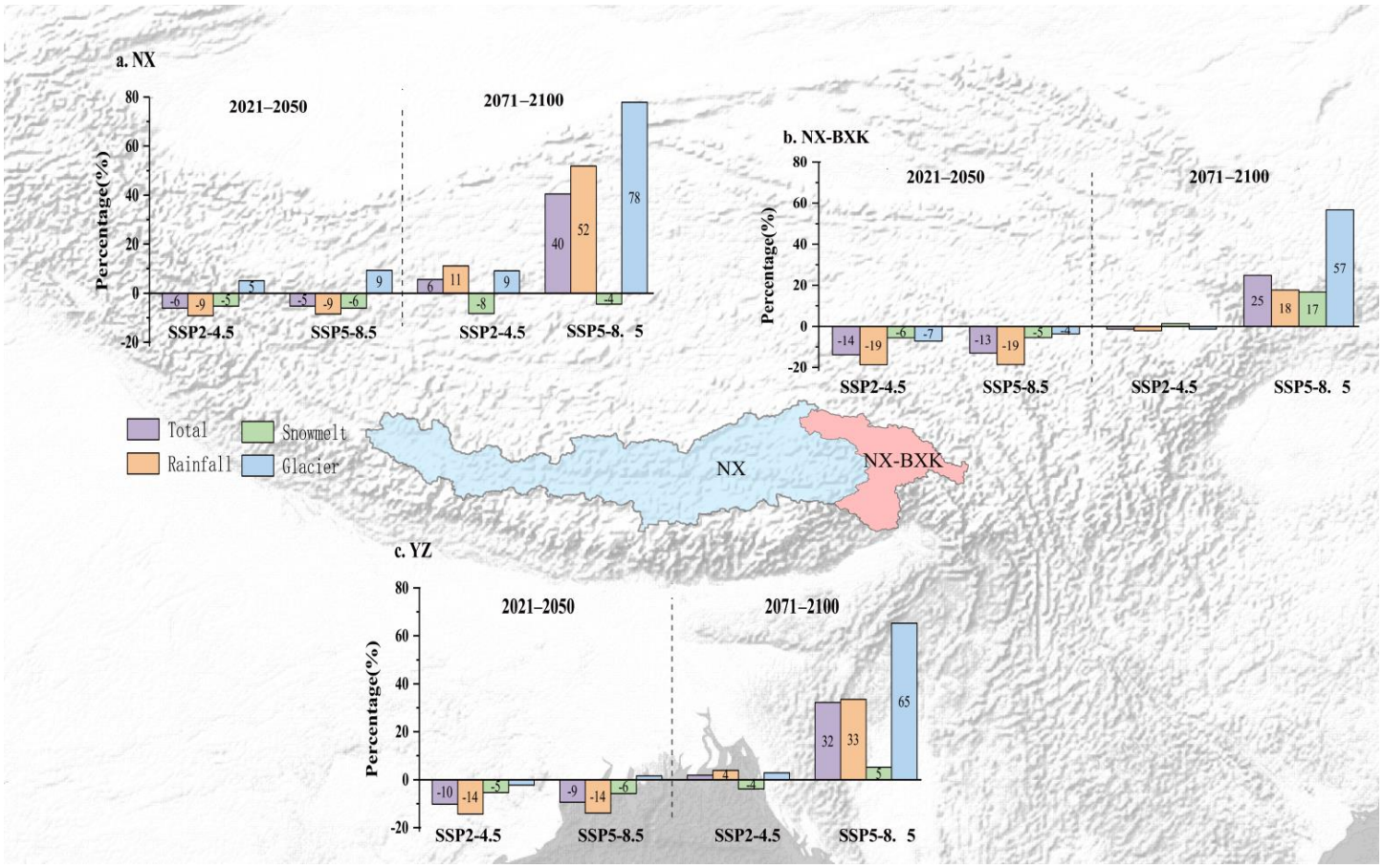

Figure 8. Projected changes (%) in the mean annual total runoff, and three runoff components (rainfall, glacier, and snowmelt) in 2021–2050 and 2071–2100, respectively, relative to 1971–2000 under the two SSPs in the YZ and its NX and NX-BXK sub-basins.

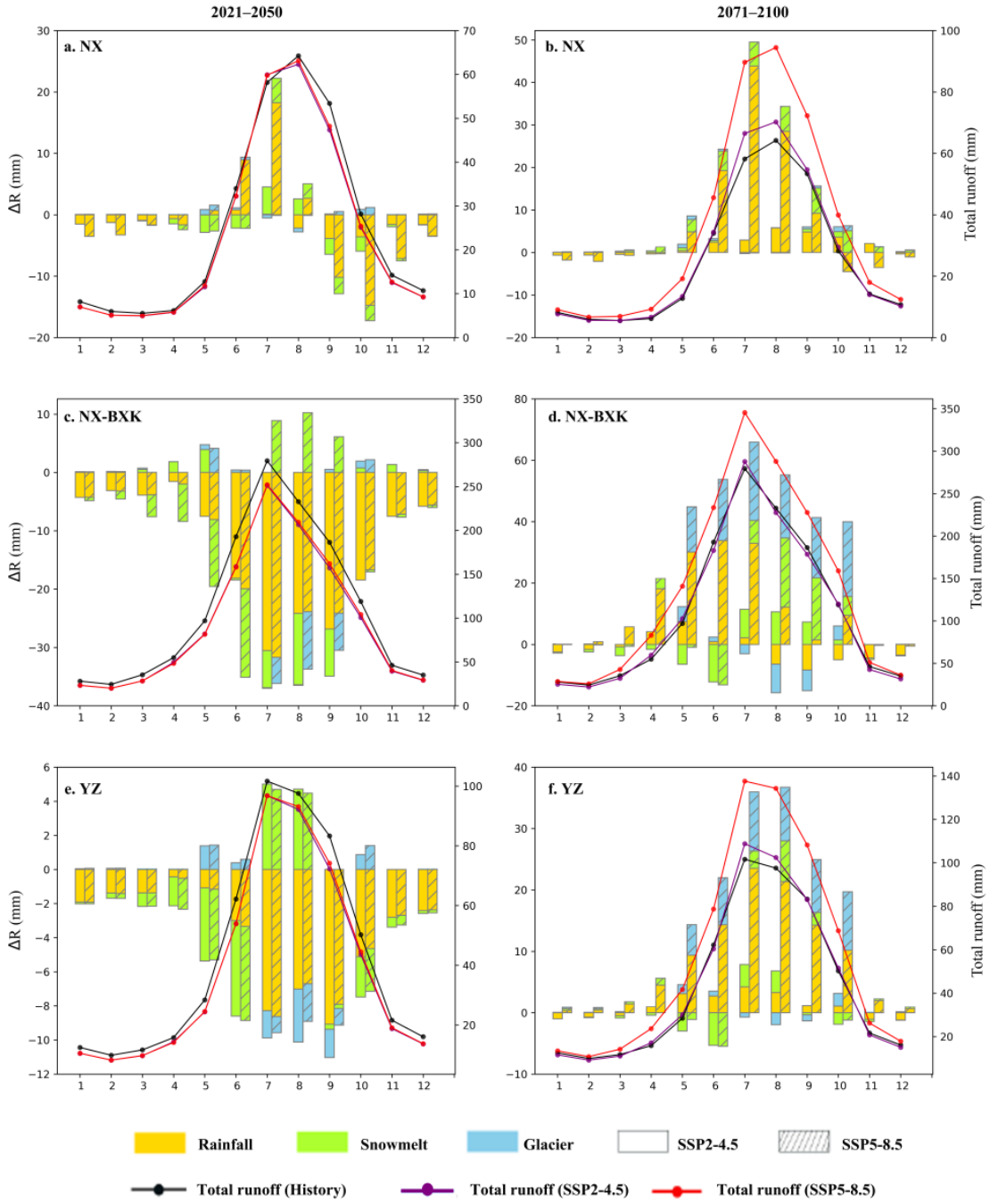

Figure 9. Monthly average of total runoff (mm) in 1971–2000, 2021–2050, and 2071–2100 and the change (mm) in their runoff components relative to 1971–2000. Dotted solid lines represent simulated mean monthly total runoff in three periods. Bar plots indicate the mean seasonal changes in rainfall, snowmelt, and glacier runoff in 2021–2050 and 2071–2100 relative to 1971–2000, based on the ensemble means of 10 hydrological simulations under the two SSPs in the YZ and its NX and NX-BXK sub-basins.

Table 1. Summary of relevant studies on simulated runoff component contributions in the YZ basin.

Basin	Runoff contribution (%)			Period	Method	Precipitation Data	References
	Glacier	Snowmelt	Rainfall				
NX	11.6	23	65.4	1961–1999	VIC+DD	Corrected CMA data	Zhang et al. (2013)
	16	9	59	1998–2007	SPHY+DD	APHRODITE	Lutz et al. 2014
	15	27.3	57.7	1971–2000	VIC+DD	Corrected CMA data	Su et al. (2016)
	9.9	10.6	79.5	2003–2014	CREST	CGDPA, TMPA	Chen et al. (2017)
	5.5	23.1	71.4	1971–2010	VIC+DD	Interpolated CMA data	Zhao et al. (2019)
	13.9	23.8	62.3	1980–2000	VIC+DD	Reconstructed data	Sun and Su (2020)
	1.8	13.2	62.1	1985–2014	SPHY+DD	ERA5	Khanal et al. (2021)
	18.4	22	69.6	2001–2010	isoGSM	CMFD	Nan et al. (2021)
	3.5–7.2	16.6–22.3	—	1981–2019	WEB-DHM	Reconstructed data	Wang et al. (2021)
NX-BXK	45.3	15.1	39.6	1980–2000	VIC+DD	Reconstructed data	Sun and Su (2020)
	5.7–8.2	7.2–7.8	—	1981–2019	WEB-DHM	Reconstructed data	Wang et al. (2021)
YZ	32.7	18.4	48.9	1980–2000	VIC+DD	Reconstructed data	Sun and Su (2020)
	5.5	17.2	73.3	1981–2019	WEB-DHM	Reconstructed data	Wang et al. (2021)

Note: VIC+DD=The Variable Infiltration Capacity (VIC) linked with a degree-day glacier melting model; SPHY+DD=The Spatial Processes in Hydrology (SPHY) linked with a degree-day glacier melting model; CREST=Coupled Routing and Excess Storage model; isoGSM=Scripps global spectral model with water isotopes incorporated; WEB-DHM= Water and energy budget-based distributed hydrological model; CMFD= China Meteorological Forcing Dataset.

Table 2. Characteristics of the six sub-basins in the Yarlung Zangbo River

		LZ	LZ-YC	RKZ	LS	YC-NX	NX-BXK	YZ
Outlet		Lhatse	Yangcun	Shigatse	Lhasa	Nuxia	Pasighat	Pasighat
Hydrological station	Name	Lhatse	Yangcun	Shigatse	Lhasa	Nuxia	Motuo	—
	Latitude (°N)	29.05	29.28	29.25	29.63	29.47	29.32	—
	Longitude (°E)	87.38	91.88	88.88	91.15	94.57	95.29	—
Drainage area (km^2)		50553	71926	11064	26235	41770	51507	253,055
Basin average elevation (m)		5370	4767	5353	5272	4937	3711	4901
Mean annual precipitation (mm) *		283	417	361	564	939	1465	774
Mean annual temperature (℃) *		-2.91	0.24	1.73	-1.28	0.97	1.21	-0.2
Glacier area (km^2)		809	640	134	257	1174	5259	8273
Glacier coverage (%) **		1.60	0.89	1.21	0.98	2.81	10.21	3.27
Snow cover area (km^2) ***		7876	7344	772	6055	10129	16467	48643
Snow cover fraction (%) ***		15.58	10.21	6.98	23.08	24.25	31.97	19.22

*The periods of precipitation and temperature data are from 1961 to 2020 (Sun et al., 2022).

**Glacier data are from the first China Glacier Inventory, http://westdc.westgis.ac.cn/glacier.

***snow cover area and snow cover fraction data are from the MODIS 10CM (2001─2019), https://nsidc.org/data

Table 3. Values of the first (D1, m), the second soil depth (D2, m) and degree-day factor (DDF), and the Nash-Sutcliffe Efficiency (NSE) and Relative Bias (RB, %) of the simulated monthly streamflow with the Variable Infiltration Capacity (VIC)-Glacier model relative to the observation for the eight hydrological stations.

Step1. Calibration and validation of the glacier model					
Sub-basin	Hydrological station	DDF ($mm°C^{-1}$ day^{-1})	Calibration (glacier area observations)	Validation (glacier mass balance)	
			RB (%)	CC	RB (%)
LZ	LZ	10.97	-1.3	0.65-0.96	-15% to -45%
LZ-YC	YC	10.97	-3.7		
RKZ	RKZ	10.97	-6.2		
LS	LS	9.2	-2		
YC-NX	NX	6.8	-1.5		
NX-BXK	YG	6.5	1.7		
	BM	6.5			
	MT	6.5			

Step2. Calibration and validation of the VIC model							
Sub-basin	Hydrological station	D1(m)	D2(m)	Calibration (observed streamflow)		Validation (observed streamflow)	
				NSE	RB (%)	NSE	RB (%)
LZ	LZ	0.1	0.7	0.85	2.1	0.81	1.8
LZ-YC	YC	0.1	0.7	0.83	3	0.81	1.6
RKZ	RKZ	0.1	0.9	0.84	-4	0.71	-8
LS	LS	0.1	0.7	0.84	-2	0.82	-2
YC-NX	NX	0.1	1	0.86	-4	0.86	-5
NX-BXK	YG	0.1	1	0.82	-8	0.83	-5
	BM	0.1	1	0.83	-6	0.83	-5
	MT	0.1	1	0.71	6	0.73	5

Table 4. Trends in precipitation, temperature, total runoff, and three runoff components and their contributions to total runoff in the YZ and its NX and NX-BXK sub-basins for different periods. Asterisks indicate the 95% confidence level.

Basin		NX			NX-BXK			YZ		
Period		1971–2020	1971–1997	1998–2020	1971–2020	1971–1997	1998–2020	1971–2020	1971–1997	1998–2020
Precipitation (mm/10yr)		11.7 *	2.9	-6.9	-35 *	52	-16.4	2.1	8.3	-8.8
Temperature (℃/10yr)		0.4 *	0.2 *	0.3 *	0.1 *	0.1	0.3 *	0.3 *	0.2 *	0.3 *
Runoff (mm/10yr)	Total	9.4 *	1.1	-3.3	-21	48.1	-0.3	3.1	8.9	-2.7
	Glacier	1.1 *	0.6	0.7	6.0 *	0.1	16.1	2.0 *	0.1	3.9
	Snowmelt	-1	0.5	-3.4	-6	20.6 *	5.7	-1.9 *	4.6 *	-1.5
	Rainfall	9.4 *	0.9	-0.6	-22	27.6	-22.1	3.0	4.9	-5.0
Contribution (%/10yr)	Glacier	-0.1	-0.2	0.3	0.8 *	-0.7	1.2	0.3	-0.4	0.8
	Snowmelt	-1.1 *	0.3	-0.8	-0.1	0.9	0.3	-0.5 *	0.6	-0.3
	Rainfall	1.1 *	-0.1	0.6	-0.7 *	-0.3	-1.6 *	0.2	-0.2	-0.5

Table 5. Trends of projected annual precipitation (mm/10 yr), temperature (°C/10 yr), and total runoff and runoff components (mm per decade) from 10 GCMs for 1971–2000, 2021–2050, and 2071–2100 under the two SSPs in the YZ and its two sub-basins (The uncertainties are indicated with one standard deviation).

		NX	NX-BXK	YZ
SSP2-4.5 2021–2050	Total runoff	6.84±4.9	52.65±22.41	16.15±7.37
	Rainfall runoff	5.53±3.97	29.99±15.43	10.54±5.73
	Snowmelt	-0.43±1.0	9.24±6.88	1.54±1.71
	Glacier runoff	1.68±1.32	13.41±6.91	4.07±2.38
	Precipitation	4.98±8.96	31.87±27.85	10.4±11.59
	Temperature	0.43±0.16	0.42±0.12	0.43±0.15
SSP5-8.5 2021–2050	Total runoff	16.22±6.78	59.34±28.23	24.99±10.59
	Rainfall runoff	11.9±5.75	31.2±22.06	15.82±8.69
	Snowmelt	1.35±1.05	9.53±5.65	3.01±1.88
	Glacier runoff	2.98±0.54	18.61±3.77	6.16±1.06
	Precipitation	18.02±11.86	32.73±36.08	21.01±16.29
	Temperature	0.66±0.1	0.6±0.09	0.64±0.09
SSP2-4.5 2071–2100	Total runoff	9.23±9.84	25.5±17.35	12.54±10.25
	Rainfall runoff	8.94±8.03	19.67±15.03	11.13±8.83
	Snowmelt	-0.03±1.36	2.12±9.24	0.41±2.01
	Glacier runoff	0.31±1.47	3.71±5.52	1±2.21
	Precipitation	11.36±12.87	23.64±21.36	13.86±12.59
	Temperature	0.32±0.2	0.27±0.15	0.31±0.19
SSP5-8.5 2071–2100	Total runoff	35.84±23.12	142.1±84.67	57.45±35.38
	Rainfall runoff	33.69±21.52	96.06±53.31	46.37±27.89
	Snowmelt	-3.63±4.7	11.07±6.32	-0.64±3.25
	Glacier runoff	5.78±4.59	34.97±27.18	11.72±9.12
	Precipitation	39.45±25.96	93.83±50.16	50.52±30.66

	Temperature	1.01±0.59	0.98±0.57	1±0.58
SSP2-4.5 2021–2100	Total runoff	7.18±2.77	34.09±9.51	12.65±3.91
	Rainfall runoff	7.23±1.89	26.78±6.02	11.21±2.53
	Snowmelt	-0.46±0.56	3.97±1.86	0.44±0.68
	Glacier runoff	0.4±0.58	3.34±2.99	1±1.06
	Precipitation	7.07±2.61	22.51±7.59	10.21±3.02
	Temperature	0.36±0.08	0.34±0.08	0.35±0.08
SSP5-8.5 2021–2100	Total runoff	27.31±10.14	100.85±30.71	42.27±13.82
	Rainfall runoff	21.41±10.14	59.17±18.38	29.09±9.53
	Snowmelt	0.14±0.63	11.96±3.7	2.55±0.96
	Glacier runoff	5.76±2.35	29.73±11.49	10.64±4.18
	Precipitation	25.34±9.39	61.86±23.92	32.77±11.26
	Temperature	0.85±0.17	0.79±0.17	0.84±0.17